NASA
Technical
Paper
1966

February 1982

Simulator Study of Vortex Encounters by a Twin-Engine, Commercial, Jet Transport Airplane

Earl C. Hastings, Jr.,
and Gerald L. Keyser, Jr.

NASA

NASA Technical Paper 1966

1982

Simulator Study of Vortex Encounters by a Twin-Engine, Commercial, Jet Transport Airplane

Earl C. Hastings, Jr.,
and Gerald L. Keyser, Jr.
Langley Research Center
Hampton, Virginia

National Aeronautics
and Space Administration

**Scientific and Technical
Information Branch**

SUMMARY

A simulator study of vortex encounters has been conducted for a twin-engine, commercial, jet transport airplane encountering the vortex flow field of a heavy, four-engine, commercial, jet transport airplane in the final-approach configuration. The encounters were conducted with fixed controls and with a pilot using a state-of-the-art, manual-control system.

Piloted encounters with the base-line vortex flow field out of ground effect (unattenuated) resulted in initial bank-angle excursions greater than 40°, coupled with initial sideslip-angle excursions greater than 10°. The severity of these initial upsets was significantly reduced when the vortex center was moved laterally or vertically away from the flight path of the encountering airplane. Smaller reductions occurred when the flow field was attenuated by the flight spoilers on the generating airplane. The largest reduction in the severity of the initial upsets, however, was from aging in ground effect. The severity of the initial upsets of the following airplane was relatively unaffected by the approach speed. Increasing the lift coefficient of the generating airplane resulted in an increase in the severity of the initial upsets.

Piloted encounters with the flow field out of ground effect resulted in large and persistent Dutch roll oscillations following the initial upset. The duration of these oscillations was 15 sec or longer and made the recovery difficult at the low encounter altitudes of these simulations. When the laterally offset location of the flow field produced a net downwash on the following airplane, the recovery was further complicated by nose-down pitching and large changes in the vertical flight path. The recovery maneuver became noticeably less difficult as the flow field aged in ground effect.

The piloted encounters were evaluated as acceptable or unacceptable by using altitude-dependent bank angle and flight-path deviation criteria. Some upsets from piloted encounters with the flow field in ground effect at an age of 120 sec were found to be acceptable at vortex-encounter altitudes of 54.9 m and 76.2 m. None of the upsets were acceptable at an encounter altitude of 30.5 m when using a criteria previously developed for a larger commercial, jet transport airplane.

INTRODUCTION

The adverse effect on landing capacity of vortex-imposed separation between airplanes has stimulated extensive research on a means of reducing these intervals. Much of this research has been concerned with the characteristics of vortices generated in flight and also with the means of reducing the severity of upsets from encounters with these vortices. These investigations have included flight tests, tests in ground facilities, and theoretical analyses. The flight-simulation technique used in this investigation has capabilities not currently available with these techniques and provides both initial upset and dynamic recovery data in six degrees of freedom with rigidly defined vortex-encounter conditions.

In the investigation discussed herein, vortex encounters were simulated with a twin-engine, commercial, jet transport airplane in the approach configuration. In the simulations, the following airplane made normal landing approaches until it passed through a vortex segment (approximately 75 m in length) on the approach path. These simulated encounters were performed with fixed controls and also with a pilot using a state-of-the-art, manual-control system. The vortex flow-field characteristics and the vortex-encounter conditions were changed parametrically, and the responses of the simulated airplane were computed and analyzed. The piloted encounters were performed in the Langley Visual/Motion Simulator.

The objective of this parametric investigation was to show the effects of lateral and vertical vortex location, vortex aging in and out of ground effect, airspeed of the following airplane, lift coefficient of the generating airplane, and vortex attenuation on the generating airplane when using flight spoilers. Partial results are presented in references 1 and 2. The purpose of this paper is to present additional data, not previously published, and to compile all of the results into a single report. This report also examines several altitude-dependent criteria for acceptable upsets and compares the simulation results with these criteria.

The values of some of the lateral-directional data given herein for centered encounters differ from those given in references 1 and 2 for the same conditions. This is a result of several recent modifications in the computer program for the vortex-induced forces and moments on the simulated airplane. These quantitative differences, however, do not invalidate any of the conclusions reached in those references. Where quantitative differences are observed, the data in this report should take precedence.

SYMBOLS

Values are given in SI units, and, where considered useful, U.S. Customary Units are supplied. Measurements and calculations were made in U.S. Customary Units.

b wing span, m

C_D drag coefficient, $\frac{\text{Drag}}{\bar{q}S}$

C_L lift coefficient, $\frac{\text{Lift}}{\bar{q}S}$

C_l rolling-moment coefficient (rolling moment positive to the right), $\frac{\text{Rolling moment}}{\bar{q}Sb}$

C_m pitching-moment coefficient (pitching moment positive with nose up), $\frac{\text{Pitching moment}}{\bar{q}S\bar{c}}$

C_n yawing-moment coefficient (yawing moment positive when nose rotates to the right), $\frac{\text{Yawing moment}}{\bar{q}Sb}$

C_{n_p} $= \frac{\partial C_n}{\partial \frac{pb}{2V}}$

C_{Y_β} variation of side-force coefficient with angle of sideslip per radian

$\bar{c}$ wing mean aerodynamic chord, m

F_X force along X_B body axis, positive forward, N

F_Y force along Y_B body axis, positive to left, N

F_Z force along Z_B body axis, positive down, N

h altitude with respect to sea level, m

h_e altitude at vortex encounter, m

Δh vertical deviation from the glide slope, m

M_X rolling moment (positive to the right), N-m (ft-lb)

M_Y pitching moment (positive with nose up), N-m (ft-lb)

M_{Y_α} variation in pitching moment with angle of attack, N-m/deg

M_Z yawing moment (positive with nose to the right), N-m (ft-lb)

M_{Z_β} variation in yawing moment with angle of sideslip, N-m/deg

m mass, kg (lb)

p roll rate about X_B-axis (positive with roll to the right), deg/sec

$\bar{q}$ free-stream dynamic pressure, Pa (lb/ft^2)

R radial distance from vortex center line, m

r yaw rate about Z_B-axis (positive with yaw to the right), deg/sec

S reference area, m^2

T vortex age, sec

t time, sec

V velocity, knots or m/sec

V_{tan} vortex tangential velocity, m/sec

X_B, Y_B, Z_B airplane body-axis system with origin at c.g. (see fig. 9)

X_E, Y_E, Z_E Earth-axis system with origin at target touchdown point (see fig. 9)

x_B distance measured parallel to X_B-axis (positive forward), m

x_E longitudinal distance between target touchdown point and c.g. (positive prior to reaching target touchdown point), km

y_B distance measured parallel to Y_B-axis (positive to right), m

y_E lateral distance between extended runway center line and c.g. (positive to right as viewed from the target touchdown point), m

y_{vor} lateral distance parallel to Y_E-axis, from c.g. to center of right-wing vortex (positive for vortex to left of c.g. as viewed from the airplane), m

Δy lateral deviation from the localizer course, m

z_B distance measured parallel to Z_B-axis (positive down), m

z_{vor} vertical distance parallel to Z_E-axis, from c.g. to center of right-wing vortex (positive for vortex below c.g.), m

α angle of attack (positive with nose up), deg

$\Delta\alpha$ vortex-induced angle of attack, deg

β angle of sideslip (positive with nose to left), deg

$\dot{\beta}$ rate of sideslip, deg/sec

$\Delta\beta$ vortex-induced angle of sideslip, deg

δ_{sp} spoiler-deflection angle on generating airplane, deg

θ body pitch attitude (positive with nose up), deg

ϕ roll attitude (positive with right wing down), deg

$\dot{\phi}$ roll rate, deg/sec

Subscripts:

c condition at vortex core

F fuselage

f the following airplane

g vortex-generating airplane

h horizontal tail

i	condition at chordwise strip of wing, vertical tail, or horizontal-tail planforms
L	left-wing vortex
max	maximum
R	right-wing vortex
t	total
v	vertical tail
vor	vortex
w	wing
Y_E	Y_E-axis direction
Z_E	Z_E-axis direction

Abbreviations:

CDI	Course Deviation Indicator
c.g.	center of gravity
IFR	Instrument Flight Rules
VFR	Visual Flight Rules
VLDS	visual landing display system
VMS	Visual/Motion Simulator

SIMULATION AND DATA ANALYSIS

SIMULATION

Simulator

The Langley Visual/Motion Simulator (VMS) used in this study is described in detail in reference 3. A photograph of the VMS is shown in figure 1. The VMS is a six-degree-of-freedom, motion-base simulator capable of presenting realistic acceleration and attitude cues to the pilot. Audio cues for engine noise and aerodynamic buffet are also provided. The simulator cockpit represents a typical, small, jet transport airplane with pilot and copilot stations. Pilot controls include the typical control wheel, pedals, and right-hand throttle quadrant. Airplane attitude-display information is provided with localizer and glide-slope pitch/roll command bars. Other instrumentation included indicated airspeed, vertical velocity, and altitude.

The visual landing display system (VLDS) in the Langley Visual/Motion Simulator shown in figure 2 provides the pilot with a colored out-the-window scene of the simulated terrain. The system utilizes an 18-m by 7.3-m (60-ft by 24-ft), three dimensionally scaled terrain model, including a large commercial airport, which is traversed in three axes by a gantry carrying a closed-circuit color-television camera. Gantry movements account for airplane spatial position, whereas the television optics-system motions account for heading, pitch, and bank of the airplane. Camera and gantry motions are commanded by the airplane-simulation computer program, and the resulting scene is routed to the window screen of the VMS.

Computer Program

Real-time simulation studies had previously been conducted in the VMS for the Boeing 737-100 airplane shown in figure 3. (Descriptions of these simulations and of some of the airplane characteristics used in the simulations are given in refs. 4 and 5.) Because of this prior simulation experience, and since this is a typical, commercial, jet transport as well, the 737-100 was used as the simulated airplane in this investigation. Table I presents the pertinent dimensional and inertial characteristics of this airplane. Aerodynamic characteristics used in this study were obtained from references 5 and 6 and from unpublished data provided by the airplane manufacturer.

A computer subroutine was written to include vortex-induced force and moment terms in the existing program. The equations used for these terms are described in the appendix of this paper and in reference 7. In addition to utilizing this subroutine in the VMS simulation of the piloted encounters, it was also integrated into an existing six-degree-of-freedom computer program to calculate the vortex-induced motions of the simulated airplane with the control surfaces fixed and the stability augmentation system inoperative. These computations were used to determine the initial vortex-induced moments and attitudes with no contribution due to control-surface motions.

Vortex Flow-Field Models

All of the flow-field models used in this investigation were for the vortex-generating airplane shown in figure 4. The first part of this section describes the vortex velocity distributions for various conditions of interest. These velocity distributions were for an isolated vortex generated by one wing of the generating airplane at various flight conditions and ages. The second part of this section discusses the manner in which these velocity distributions were used to define the three-dimensional flow-field models (including both vortices) used in the simulations.

Velocity distributions for isolated vortices.- Table II lists the six conditions for which velocity distributions for isolated vortices were calculated. These velocity distributions were developed by using the methods of reference 1 and are shown in figures 5 to 8. It should be noted in table II that whenever supporting data were available, velocity distributions were determined for four vortex ages (T = 45, 60, 90, and 120 sec). These vortex ages represented separation intervals of 3.24 km (1.75 n. mi.), 4.32 km (2.33 n. mi.), 6.48 km (3.50 n. mi.), and 8.65 km (4.67 n. mi.) for V_g = 140 knots. The separation interval corresponding to T = 120 sec is approximately the same as that currently required in flight operations involving the leading and following airplanes simulated in this investigation.

The base-line vortex is for the generating airplane in the normal landing-approach configuration (wing leading- and trailing-edge flaps deployed, all landing flaps at 30°, landing gear down, $C_{L,g} = 1.40$, and $V_g = 140$ knots). Except where noted, the mass of the generating airplane was 231 293 kg (509 914 lb). The base-line vortex was modeled for two conditions. The first condition, "base-line vortex out of ground effect," is for the condition where the vortex is not significantly influenced by the effect of the ground plane. The second condition, "base-line vortex in ground effect," is where the same vortex had descended to a height where the presence of the ground plane has significantly affected both the tangential velocities and the rate of descent of the vortex. This effect is discussed in detail in reference 8. Various tests, including those in reference 8, have indicated that for the generating airplane used here, ground effect became significant when the flow field had descended to a height between about 25 and 45 m above the ground plane.

Figure 5 shows the velocity distributions calculated for the two base-line conditions. These data were determined by using the methods described in reference 1. The velocity distributions out of ground effect (fig. 5(a)) are characterized by large values of V_{tan} near the core radius R_c (where R_c is at $V_{tan,max}$). These large values of V_{tan} decrease relatively rapidly between $R = R_c$ and $R \approx 6$ m. Beyond $R \approx 6$ m, the decrease in V_{tan} with both increasing R and increasing T is more gradual. The velocity distributions in ground effect (fig. 5(b)), however, show reduced values of V_{tan} near R_c. These values decrease gradually with increasing R beyond $R \approx 6$ m, and there is a significant decrease in V_{tan} with increasing T. The core radius is also noted to be larger in ground effect than out of ground effect.

The vortex conditions in table II, denoted "high $C_{L,g}$" and "low $C_{L,g}$," were for the generating airplane at approach lift coefficients of 1.54 and 0.98, respectively, rather than at $C_{L,g} = 1.4$ as in the base-line conditions. The changes in $C_{L,g}$ from the nominal value were achieved by increasing and decreasing the nominal mass of the generating airplane, while maintaining the same approach speed, and will be discussed in more detail later. At both of these values of $C_{L,g}$, the velocity distributions were calculated (by using the method of ref. 1) for the vortex out-of-ground-effect condition.

Figures 6 and 7 show the velocity distributions for the high $C_{L,g}$ and low $C_{L,g}$ conditions, respectively. The velocity distributions for the high $C_{L,g}$ condition have trends similar to the base-line data out of ground effect, although these values of V_{tan} are slightly greater than the base-line values. The velocity distributions for the low $C_{L,g}$ condition, however, have significantly lower values of V_{tan} at all values of R, and the largest values are all located at values of R less than about 6 m.

The vortex conditions in table II denoted "Attenuated (15° spoilers)" and "Attenuated (30° spoilers)" were for the generating airplane in the normal landing-approach configuration, with spoilers 2, 3, and 4 (see fig. 4) deployed at $\delta_{sp} = 15°$ and 30° for vortex attenuation. The velocity distributions for these conditions are shown in figure 8. Note that, for the 15° spoiler condition (fig. 8(a)), distributions are shown only for $T = 60$ sec and 90 sec and that, for the 30° spoiler condition (fig. 8(b)), distributions are shown only for $T = 45$ sec and 60 sec. These distributions were all determined as described in reference 1. It should also be noted that all of the data shown in figure 8 apply both in and out of ground effect since the measurements upon which they were based (see ref. 1) showed no enhanced alleviation in ground effect.

The velocity distributions in figure 8(a) for $\delta_{sp} = 15°$ show trends similar to the base-line in-ground-effect data (fig. 5(b)) at $T = 60$ sec and 90 sec. In comparison to the unattenuated vortices, values of V_{tan} are greatly reduced near R_c and decrease significantly with increasing R and increasing T. The data in figure 8(b), however, show that for $\delta_{sp} = 30°$, V_{tan} decreases very slowly with increasing values of R between $T = 45$ sec and 60 sec. It can also be noted that the velocity distributions at both vortex ages are nearly the same, with the older vortex actually appearing stronger. As noted in reference 1, these distributions were determined from a limited amount of test data and, although used as shown, they are taken to indicate only that the vortex decayed very slowly between $T = 45$ sec and 60 sec.

Three-dimensional flow-field models.- The test technique used in the investigation was, in effect, to impose a short-duration vortex pulse on the simulated airplane and analyze the resultant response after the vortex pulse was removed. Figure 9 shows the approach geometry, the Earth- and body-axis systems, and a typical flow-field model used in this investigation. The figure shows that each flow field had a length determined by the longitudinal distance between vertical entry and exit plane. Each three-dimensional flow-field model was composed of two counterrotating vortices having centers along the lines indicated in the figure. It was assumed that, for any combination of vortex conditions and age (table II), the velocity distribution about both vortex centers was the same and they were invariant along the segment length.

The lateral distance between the vortex centers was 42.1 m. This spacing is about 70 percent of the span of the generating airplane. This spacing was taken from unpublished experimental results from the Langley Vortex Research Facility which used a 0.03-scale model of the generating airplane in the approach configuration. The length of the flow field used in all of the simulations was 76.2 m. This value was also determined experimentally and differs from the 122-m length used in references 1 and 2. As a result of changes in the subroutine which calculates vortex-imposed forces and moments, the flow-field length was adjusted to correlate with flight-test bank-angle data contained in an appendix of reference 1. The 76.2-m flow-field length was chosen as the one giving the best agreement between the data and the simulations and corresponds to a nominal encounter time of 1.18 sec.

Although this method of flow-field modeling is felt to be suitable for this parametric investigation, it is recognized that flow-field effects such as internal turbulence and vortex meander have not been included. For these and other reasons, these flow-field models should not be taken as precise representations of those of the generating airplane.

The flow-field models were located relative to an Earth-fixed reference system centered at the target touchdown point 305 m from the runway threshold. (See fig. 9.) Moving the flow-field model laterally or vertically changed the location of the vortex centers relative to the flight path of the airplane at a given encounter altitude. Moving the flow field along the 3° glide-slope line changed the vortex-encounter altitude. Unless noted otherwise, the centered (reference) encounter condition in this study ($y_{vor} = 0$, $z_{vor} = 0$) was for the simulated airplane located in the center of the right-wing vortex of the generating airplane.

The sketch in figure 9 also illustrates how the effect of both vortices was calculated. At any point in the flow field, the lateral and vertical components of the resultant tangential velocity were the sum of the components of the right and left vortices at that point and are given as follows:

$$\left(V_{tan}\right)_{Y_E} = \left(V_{tan}\right)_{Y_{E,L}} + \left(V_{tan}\right)_{Y_{E,R}} \tag{1}$$

$$\left(V_{tan}\right)_{Z_E} = \left(V_{tan}\right)_{Z_{E,L}} + \left(V_{tan}\right)_{Z_{E,R}} \tag{2}$$

This computational procedure is discussed in more detail in the appendix and in reference 7.

Test Procedure

In the fixed-control simulations, the airplane was trimmed at the desired conditions and flew an undisturbed, 3° glide slope toward the projected touchdown point. The stability augmentation system (yaw damper) of the airplane was not operative in these simulations. Following the vortex flow-field encounter, the airplane flight was computed with controls fixed until the run was terminated near the ground. In the piloted simulations, the pilot manually flew instrument approaches along the glide slope toward the target touchdown point. The stability augmentation system was operative in these simulations. Following the flow-field encounter, the pilot used both instrument information and outside visual cues to regain control of the airplane and attempt to complete the landing.

The effect of variations in pilot technique was not studied in this investigation. However, to minimize the possible influence of this effect, the same research test pilot was used in all of the piloted simulations discussed herein, and the same recovery technique was used to the greatest extent possible. In general, the recovery technique found most suitable for piloted encounters with the stronger flow fields (i.e., base-line flow field out of ground effect) involved several, nearly simultaneous, control inputs. Full aileron deflection against the roll was usually required. Although the strong flow fields usually produced severe sideslip, the rudder was generally not used early in the recovery in order to avoid the possibility of further exciting the Dutch roll oscillations. Pitch-attitude changes and vertical-path changes also resulted from some encounters and required large elevator inputs simultaneously with the large aileron inputs. During the recovery maneuver, power was frequently added in an open-loop fashion during the upset, and then it was reset based on engine-noise level a short time later if no significant glide-slope deviation had occurred. The simulated runway was 3.05 km long and 61 m wide. Because of the runway length, long landings were possible and were frequently utilized as part of the recovery technique in this investigation.

The investigation was conducted with the test-condition matrix shown in table III. For the fixed-control encounters, it was always possible to place the airplane at the specified entry positions of y_{vor} and z_{vor} shown in table III. As a result of small pilot-control inputs along the nominal flight path, this was not always possible for the piloted encounters. Therefore, where not noted otherwise, the piloted-encounter data were obtained at the specified entry locations with errors not exceeding ±2 m.

DATA ANALYSIS

The data were analyzed to evaluate the effect of the various flow-field models and their locations on (1) the severity of the initial upset immediately following the vortex encounter, and (2) the airplane attitudes and flight-path excursions during the recovery maneuver following the initial upset. A third analysis involved a comparison of the initial bank angles and flight-path changes with altitude-dependent criteria which were established only for the purpose of evaluating the relative severity of upsets during these simulation studies. The first analysis was done for both fixed controls and piloted encounters, and the second and third analyses were done for piloted encounters only.

The severity of the initial upset was evaluated primarily with the parameters $C_{l,max}$, $\dot{\phi}_{max}$, ϕ_{max}, $C_{n,max}$, $\dot{\beta}_{max}$, and β_{max}. Some analyses of the initial upset also included the parameters $\Delta C_{L,vor}$ and $\Delta C_{m,vor}$. Figure 10 illustrates how these data were obtained. Although the data in this figure are from a piloted encounter, the data-analysis method also applies to encounters with fixed controls.

Figure 10 shows that the values of $C_{l,max}$, $\dot{\phi}_{max}$, ϕ_{max}, $C_{n,max}$, $\dot{\beta}_{max}$, and β_{max} were all read from the records at the first peak of the vortex-induced oscillation. The time sequence of these data was that the moment coefficients ($C_{l,max}$ and $C_{n,max}$) occurred first, the velocities ($\dot{\phi}_{max}$ and $\dot{\beta}_{max}$) occurred next, and the attitudes (ϕ_{max} and β_{max}) occurred last. All of these data were generally obtained within 4.5 sec of the vortex encounter. The parameters $\Delta C_{L,vor}$ and $\Delta C_{m,vor}$ were defined as the difference between the trimmed values prior to the encounter and the initial values when the simulated airplane was completely in the vortex segment (approximately 0.4 sec later). Vortex-induced changes in pitch attitude and flight path were negligible over this time interval. To obtain the initial upset data for the piloted encounters, each condition of interest in table III was simulated two or more times and the largest recorded values of the upset parameters were used in the analysis.

The recovery maneuver following the initial upset was evaluated by using time histories of attitudes, control deflections, and flight-path excursions. Pilot comments recorded immediately after each run were also used in evaluating the recovery maneuvers.

RESULTS AND DISCUSSION

This part of the paper is divided into seven sections, with each section dealing with a separate study. The sections are as follows:

EFFECT OF LATERAL LOCATION OF FLOW FIELD
EFFECT OF VERTICAL LOCATION OF FLOW FIELD
EFFECT OF VORTEX AGING
EFFECT OF AIRSPEED OF THE FOLLOWING AIRPLANE
EFFECT OF LIFT COEFFICIENT OF THE GENERATING AIRPLANE
EFFECT OF FLIGHT SPOILERS AS VORTEX ATTENUATORS
ACCEPTABLE UPSETS

In this report, the base-line flow field out of ground effect, at a vortex age of 120 sec (fig. 5(a)), is often used for making data comparisons since these conditions represent those of the unattenuated flow field of this generating airplane at a separation interval close to that currently required in flight operations.

EFFECT OF LATERAL LOCATION OF FLOW FIELD

In studying the effect of lateral location of the flow field, data were obtained from simulated encounters with the base-line flow field out of ground effect at $T = 120$ sec with the lateral displacements shown in table III. As a result of the entry errors in the piloted encounters, however, the data were obtained and plotted at values of y_{vor} which differ slightly from those listed in table III. In this study, $z_{vor} = 0 \pm 2$ m. The results of this study are given in figures 11, 12, and 13.

The effect of the lateral location of the flow field on the initial upset is shown in figure 11. The lateral-directional upset parameters are shown in figure 11(a), and the longitudinal upset parameters are shown in figure 11(b).

The roll parameters ($C_{l,max}$, $\dot{\phi}_{max}$, and ϕ_{max}) in figure 11(a) show that the most severe roll upsets occurred at about $y_{vor} = 0$ where the simulated airplane was centered with the right-wing vortex. The severity decreased in a generally symmetrical manner as the flow field moved laterally left or right of this reference position. The variation of $C_{l,max}$, $\dot{\phi}_{max}$, and ϕ_{max} with y_{vor} was almost totally due to the decreasing influence of the right-wing vortex on the wing of the simulated airplane.

The data from the piloted encounters show that the use of the controls by the pilot reduced both $\dot{\phi}_{max}$ and ϕ_{max} at all values of y_{vor}. These data also show that moving the flow field laterally from $y_{vor} = 0$ to $y_{vor} = \pm 8$ m reduced ϕ_{max} from -40° to about -17°. Although this reduction in ϕ_{max} was significant, the values of ϕ_{max} at $y_{vor} = \pm 8$ m were still considered too large to be acceptable at low altitudes. Acceptable bank-angle criteria are discussed later in this paper.

The values of the directional parameter $C_{n,max}$ in figure 11(a) show the same trend as the roll parameters. An analysis of the calculated aerodynamic and vortex-induced yawing moments indicated that the major contributor to the value of this parameter was the aerodynamic C_{n_p} of the basic airplane (as opposed to the vortex-induced yawing moments). It was, in fact, observed that positive (nose right) values of $C_{n,max}$ always occurred for negative (left wing down) roll regardless of the direction of the vortex-induced crossflow on the vertical tail.

Unlike the other data in figure 11(a) the directional parameters $\dot{\beta}_{max}$ and β_{max} varied asymmetrically with y_{vor} for the encounters with fixed controls. The $\dot{\beta}_{max}$ data indicate a large increase in magnitude for values of y_{vor} between about -3 m and 3 m, and the most severe initial, directional upset occurred at $y_{vor} = 3$ m. The β_{max} data follow the same general trend. It was found that this

effect resulted from kinematic coupling between α and β when the airplane rolled about the X_B-axis at high angles of attack. (See ref. 9.) In reference 9, the rate of sideslip generated due to kinematic coupling was given by the equation

$$\dot{\beta} \approx p \sin \alpha - r \cos \alpha \tag{3}$$

Calculations established that the difference between the values of $\dot{\beta}_{max}$ at $y_{vor} = -3$ m and 3 m in figure 11(a) was almost entirely due to differences in the values of α when $\dot{\beta}_{max}$ occurred.

The directional data in figure 11(a) from piloted encounters show that, when the pilot applied controls against the initial upset, the variations in $\dot{\beta}_{max}$ and β_{max} were more symmetrical and the maximum value was reduced slightly. These data also show that moving the flow field laterally at values of y_{vor} from 0 to ±8 m decreased β_{max} from about -10° to about -5°.

The effect of the lateral location of the flow field on the initial longitudinal upsets is shown in figure 11(b). The $\Delta C_{L,vor}$ parameter shows that when the simulated airplane, with fixed controls, was centered with the right-wing vortex at $y_{vor} = 0$, there was a reduction in C_L because of downwash from the left-wing vortex. As the flow field moved to the right of this reference position, the downwash increased and $\Delta C_{L,vor}$ became more negative. Conversely, moving the flow field to the left produced upwash and $\Delta C_{L,vor}$ became less negative. It was observed that the effect of the flow field on the horizontal tail was small and the flow-field-induced changes in lift on the wing were predominant.

The lateral location of the flow field at $y_{vor} \neq 0$ produced a change in the pitching moment as well as a change in the lift of the simulated airplane. The value of the pitching-moment parameter $\Delta C_{m,vor}$ in figure 11(b) was influenced by the flow-field effects on the horizontal tail, the fuselage, and the wing of the simulated airplane. The data indicate that, except very near $y_{vor} = 0$, the vortex-induced pitching moments from the wing and fuselage were destabilizing and overpowered the stabilizing vortex effect from the horizontal tail. The combined effect is seen to produce negative values of $\Delta C_{m,vor}$ in predominant downwash (at negative values of y_{vor}) and positive values of $\Delta C_{m,vor}$ in predominant upwash (at positive values of y_{vor}). The peak values of $\Delta C_{m,vor}$ occur at $y_{vor} \approx \pm 3$ m where the peak tangential vortex velocities are located near the fuselage reference point at the center of gravity.

The data from the piloted encounters show that, unlike the lateral-directional response data shown previously, the pilot had little control over $\Delta C_{L,vor}$ or $\Delta C_{m,vor}$ since these parameters occurred prior to the effective application of controls. It will be shown that, for laterally offset encounters, the $\Delta C_{L,vor}$ effect resulted in changes in the vertical flight path and the $\Delta C_{m,vor}$ effect resulted in initial changes in the body pitch attitude following the initial upsets.

Figure 12 shows the horizontal and vertical projections of the flight path following piloted encounters with the flow field located at $y_{vor} = 3.4$ m, 0.4 m, and -2.6 m. These locations were chosen for illustration because $\Delta C_{m,vor}$ was

largest near $y_{vor} = \pm 3$ m and because $y_{vor} = 0.4$ m represents a centered encounter with the right-wing vortex. The encounter altitudes were all at 61.0 m.

The data in figure 12(a) show that the horizontal-path deviations were all to the left of the extended runway center line (when viewed from the airplane), with the largest deviation being about 35 m. These deviations were associated with the vortex-induced roll and did not represent a serious recovery problem. Following the typical left roll resulting from encounters with the right-wing vortex, the pilot initially rolled the airplane back to a wing's level position. This was followed by a right-roll command as required to realign the airplane with the extended runway center line. After realignment, the landing was accomplished. The realignment maneuver occasionally took enough time to cause the landing to be somewhat longer than normal.

The data in figure 12(b) show that some laterally offset vortex locations resulted in very significant vertical-path changes. These changes were associated largely with the $\Delta C_{L,vor}$ effect and were much more serious than the horizontal-path changes shown in figure 12(a). The data in figure 12(b) show that, at $y_{vor} = 0.4$ m and -2.6 m (where vortex downwash resulted in negative $\Delta C_{L,vor}$ values), there was a steepening of the vertical path after the encounter. The effect was strongest at $y_{vor} = -2.6$ m where the negative value of $\Delta C_{L,vor}$ was greatest. The maximum rates of descent experienced by the simulated airplane were 8.5 m/sec for $y_{vor} = 0.4$ m and 11.6 m/sec for $y_{vor} = -2.6$ m as compared with the nominal descent rate of 3.8 m/sec. In the latter case, the airplane experienced a total altitude loss of 29.6 m in the first 5 sec following the vortex encounter.

Following the encounters at $y_{vor} = -2.6$ m and 0.4 m, the pilot applied full, or nearly full, nose-up elevator deflection to counter the nose-down pitch and vertical displacement of the airplane below the desired glide slope. The recovery technique following the encounter at $y_{vor} = 3.4$ m differed, however, since at this lateral offset there was a nose-up pitching moment and a slight displacement of the airplane above the desired glide slope. In this recovery, a full nose-down input was not made because the airplane was so close to the ground. The recovery technique in this situation was to make a slight nose-down pitch input and accept the condition above glide slope prior to landing. In some encounters, this technique resulted in slightly longer landings than usual.

Figure 13 shows histories of the angles ϕ, β, and θ following encounters at $y_{vor} = 3.4$ m, 0.4 m, and -2.6 m. The shaded bands indicate the time that the simulated airplane was in the flow field.

The ϕ and β data in figure 13 show the presence of large Dutch roll oscillations following the encounters. The large β oscillations were found to be very difficult to counter without the possibility of getting in phase with the oscillation and amplifying it. Therefore, the recovery technique was to avoid rudder inputs early in the recovery and allow the airplane's natural lateral-directional stability to damp the β oscillations to near zero. At these low encounter altitudes, this recovery technique frequently required that the flight path be flattened out in order to gain the time required for the oscillation to damp out. This frequently resulted in a rather long landing. Because of these considerations, persistent Dutch roll oscillations such as those in figure 13 were regarded as a serious vortex-recovery problem at the encounter altitudes in this investigation.

The θ histories in figure 13 show the vortex-induced pitch effect noted earlier. At $y_{vor} = 0.4$ m there was very little initial change in θ, but there was an initial nose-up pitch when $y_{vor} = 3.4$ m and an initial nose-down pitch when $y_{vor} = -2.6$ m. The values of $\theta_{max} = 11°$ for $y_{vor} = -2.6$ m and of $\theta_{max} = 6°$ for $y_{vor} = 0.4$ m are the result of the large, nose-up, pilot inputs noted earlier.

EFFECT OF VERTICAL LOCATION OF FLOW FIELD

In studying the effect of vertical location of the flow field, data were obtained from simulated encounters with the base-line flow field out of ground effect at $T = 120$ sec for the vertical locations shown in table III. Because of the entry errors noted previously, the data for the piloted encounters were obtained for values of z_{vor} which differ slightly from those in the table. For this study, $y_{vor} = 0 \pm 2$ m. The results are shown in figures 14, 15, and 16.

The effect of the vertical location of the flow field on the initial upset is shown in figure 14. The roll parameters $C_{l,max}$, $\dot{\phi}_{max}$, and ϕ_{max} for the encounters with fixed controls (fig. 14(a)) show that the initial upset was most severe for a centered encounter at $z_{vor} = 0$. The severity decreased as the flow field moved vertically from this reference position. These roll parameters had slightly larger values at some positive values of z_{vor} than at corresponding negative values of z_{vor}. This was because the vortex crossflow on the vertical tail produced rolling moments which opposed those of the wing at negative z_{vor} and added to those of the wing at positive values of z_{vor}.

In figure 14(a), the directional-response parameters $C_{n,max}$, $\dot{\beta}_{max}$, and β_{max} for encounters with fixed controls show that the directional upset was strongest between about $z_{vor} = 0$ and -3 m. This occurred because, between values of z_{vor} of 0 and -4.3 m, the vortex crossflows at the vertical tail and at the fuselage reference point (c.g.) were in opposite directions, with the result that they both produced yawing moments in the same (nose right) direction. It was also observed that, although the yawing moment from the vortex flow on the vertical tail did change direction at $z_{vor} = -4.3$ m, the resultant yawing moment was always nose right. This was largely due to the previously noted influence of the aerodynamic C_{n_p} term.

The data in figure 14(a) also show that the use of controls by the pilot resulted in significant reductions in ϕ_{max} and β_{max} at all values of z_{vor}. Moving the flow field vertically from $z_{vor} = 0$ to ± 8 m reduced the value of ϕ_{max} from $-40°$ to about $-18°$ and the value of β_{max} from $-10°$ to about $-4°$. These reductions with changing z_{vor} are about the same as those noted in the preceding study for changing y_{vor}. The values of ϕ_{max} at $z_{vor} = \pm 8$ m are considered too large to be acceptable at low altitudes as will be discussed in detail later.

The effect of vertical location of the flow field on the initial longitudinal upsets is shown in figure 14(b). For comparative purposes, the $\Delta C_{L,vor}$ and $\Delta C_{m,vor}$ parameters are plotted to the same scale as the lateral-location data in figure 11(b). It is evident that these values were small at all values of z_{vor} and that, unlike lateral displacement, vertical flow-field displacement did not significantly affect the trim lift or pitching moments of the simulated airplane.

Figure 15 shows the flight-path characteristics for flow-field encounters at z_{vor} = 5.4 m, 1.2 m, and -5.0 m. The horizontal-path characteristics are generally similar to those shown in figure 12 for lateral offsets. The vertical-path projections, however, show that these data were not significantly affected by the vertical movements of the flow field. This is a result of the small $\Delta C_{L,vor}$ values (fig. 14(b)) associated with these encounters.

Figure 16 shows histories of ϕ, β, and θ following encounters with the base-line flow field at z_{vor} = 5.4 m, 1.2 m, and -5.0 m. The time that the simulated airplane was in the flow field is shown by the shaded band. The data show that the initial upset values of ϕ_{max} and β_{max} were reduced by the flow-field offset. The data also show, however, that, even with the smaller initial upset values, the typically large and persistent Dutch roll oscillations were present. Although the characteristics of the ϕ and β data in figure 16 are similar to the laterally offset data in figure 13, it is apparent that the effect of the initial encounter on θ was less severe.

The data in figures 15 and 16 are consistent with the pilots' observations of the recovery from vertically offset encounters. Although the Dutch roll oscillations were observed to be severe, the pitch-attitude changes were small and easily managed, and the rapid negative displacement of the airplane below the glide slope was mercifully absent in these encounters.

EFFECT OF VORTEX AGING

In studying the effect of vortex aging, the data were obtained from centered encounters with the base-line flow field at vortex ages of 45, 60, 90, and 120 sec. (See table III.) Figure 17 shows the effect of aging on the initial upset for encounters with the base-line flow field out of ground effect. The data from the encounters with fixed controls show that the severity of the initial roll upset (as indicated by $C_{l,max}$, $\dot{\phi}_{max}$, and ϕ_{max}) decreased about 12.5 percent between T = 45 sec and 120 sec. The decrease in $C_{n,max}$ was about 30 percent between T = 45 sec and 120 sec and resulted from a decrease in the effect of the vortex crossflow velocity on the vertical tail with increasing vortex age. The changes in $\dot{\beta}_{max}$ and β_{max} with vortex age were relatively small for encounters with fixed controls.

The data in figure 17 for the piloted encounters show that the upset parameters were generally less for the piloted encounters than with fixed controls. These data also show that, as the vortex aged from T = 45 sec to 120 sec, ϕ_{max} decreased from -48° to -40° and β_{max} decreased from -11.5° to -10°. The initial upsets shown here for T = 45 sec were observed to be the most severe of all the piloted encounters in the investigation.

The effect of vortex aging on the initial upsets for encounters with the base-line flow field in ground effect is shown in figure 18. The data from the encounters with fixed controls show that all of the initial upset parameters showed very large decreases between T = 45 sec and 120 sec. This result shows that the effect of increasing vortex age on decreasing the severity of the initial upset was much more pronounced when the flow field was in ground effect than when out of ground effect (fig. 17). The data in figure 18 for the piloted encounters show the same trend as the data for encounters with fixed controls, but at generally reduced levels of

severity. The data from the piloted encounters show that, as T increased from 45 sec to 120 sec, ϕ_{max} decreased from -42° to -11° (74 percent) and β_{max} decreased from -11.5° to -3.2° (72 percent).

The effects of vortex aging shown in figures 17 and 18 are consistent with the characteristics of the velocity distributions shown in figure 5. At $T = 45$ sec, the velocity distribution at values of R greater than about 10 m was about the same with or without ground effect. Thus, the roll upsets were similar for this vortex age. Figure 5(b), however, shows large reductions in V_{tan} for $T > 60$ sec at all values of R. This accounts for the more rapid decrease in initial roll upset with aging in ground effect.

It was also noted that the time histories following the initial upsets were significantly different. This is illustrated by the data in figure 19 where time histories of ϕ, β, and θ are compared for centered encounters (at $T = 120$ sec) in ground effect at $h_e = 30.5$ m and out of ground effect at $h_e = 61.0$ m. It is important to note that the duration of the vortex-induced Dutch roll oscillation was reduced from about 19 sec to about 8 sec. These reductions in the magnitude and in the duration of this oscillation resulted in these encounters (i.e., base-line flow field in ground effect at $T = 120$ sec) being the mildest and most easily managed in the investigation.

It was observed during this analysis, and during the analyses of other centered encounters to be discussed later, that the flight-path characteristics were all quite similar and appeared very much like that shown for the centered encounter in figures 12 and 15. Therefore, in this and subsequent parts of the paper dealing with centered encounters, flight-path data are not shown.

EFFECT OF AIRSPEED OF THE FOLLOWING AIRPLANE

As shown in table III, the flow field and the values of $C_{L,g}$ and V_g used in this study were the same as those of the preceding simulations. In these centered vortex encounters, however, the approach speed of the following airplane V_f was increased from 125 knots to 140 knots. There was a corresponding decrease in $C_{L,f}$ from 1.62 to 1.30 as a result of this change. This increased approach speed, although considerably higher than normal, was not considered unreasonable for this simulated airplane under some operating conditions.

Increasing V_f was observed to reduce the vortex-induced angles of attack and sideslip, increase the dynamic pressure, and reduce the vortex exposure time of the simulated airplane. The data in figure 20 show that, for encounters with fixed controls, there were reductions in $C_{l,max}$ and $C_{n,max}$ resulting from the lower induced angles of attack and sideslip at $V_f = 140$ knots. However, the increased dynamic pressure at $V_f = 140$ knots resulted in increased values of $\dot{\phi}_{max}$ and ϕ_{max}. The decrease in the vortex exposure time (from 1.18 sec to 1.06 sec) did not have a significant effect on these initial upsets.

The decrease in $\dot{\beta}_{max}$ at $V_f = 140$ knots resulted from the kinematic coupling effect, discussed earlier, since the initial trim values of α were not the same at the two airspeeds. This decrease in $\dot{\beta}_{max}$ with increasing V_f resulted in a corresponding decrease in β_{max} at values of V_f between 125 knots and 140 knots.

The data from piloted encounters in figure 20 show that the severity of the initial upset was relatively insensitive to the increase in V_f. Body motions are shown in figure 21 for the encounters at V_f = 125 knots and 140 knots. It can be noted that, although the two values of ϕ_{max} and the two values of β_{max} were about the same, the time required to damp out the Dutch roll oscillation was reduced by about 5 sec at the higher approach speed. This is attributed to increased control effectiveness and increased vertical-stabilizer effectiveness. Even with this favorable effect, however, the time required to damp out the vortex-induced motion was about 15 sec and was considered too long at low altitudes.

EFFECT OF LIFT COEFFICIENT OF THE GENERATING AIRPLANE

For this study, flow-field models out of ground effect were constructed by using the velocity distributions shown in figures 6 and 7 at T = 120 sec. These models were for the generating airplane with approach lift coefficient of 1.54 and 0.98, respectively. In order to maintain a consistent value of V_g = 140 knots in all of these studies, the high and low values of $C_{L,g}$ were obtained by changing the mass of the generating airplane. As shown in table III, the high $C_{L,g}$ value of 1.54 corresponds to a mass of 255 826 kg, which is equivalent to the maximum landing weight of the generating airplane. The low $C_{L,g}$ value of 0.98 corresponds to a mass of 161 978 kg, which is equivalent to the empty operating weight of the generating airplane.

The initial-upset data from encounters with fixed controls are shown in figure 22. Since the primary test pilot was not available for these particular simulations, these piloted results (obtained by using an alternate pilot) are not shown because of the possible influence of variations in pilot technique noted earlier.

The data in figure 22 show that reducing $C_{L,g}$ from the nominal value of 1.40 to the minimum value of 0.98 generally resulted in very significant reductions in the severity of the initial upset (a 33-percent decrease in ϕ_{max} and a 29-percent decrease in β_{max}). Even with this reduction, however, ϕ_{max} was still unacceptably large as will be shown later. Increasing $C_{L,g}$ from 1.40 to the maximum value of 1.54 is seen to result generally in a significant increase in the severity of the initial upset.

EFFECT OF FLIGHT SPOILERS AS VORTEX ATTENUATORS

Data in reference 10 indicated that a significant reduction in $C_{l,max}$ might occur for the simulated airplane if the generating airplane approached with flight spoilers 2, 3, and 4 extended as vortex attenuators. Therefore, simulations were performed by using the spoiler-attenuated velocity distributions shown in figure 8. As noted earlier, these distributions apply either in or out of ground effect since the measurements upon which they were based showed no enhanced alleviation in ground effect.

Figure 23 shows the results from encounters with the flow field of the generating airplane with the spoilers extended. The effectiveness of the spoilers as vortex-attenuating devices was found by comparison of the fixed-control data with spoilers with the fixed-control data for the base-line flow field out of ground effect. In figure 23 the base-line data are shown by the dashed lines and are taken from figure 17.

The fixed-control data in figure 23(a) show that at $T = 60$ sec and 90 sec, the 15° spoilers generally resulted in reduced initial upsets. At $T = 60$ sec, the use of 15° spoilers reduced ϕ_{max} by about 10° and β_{max} by about 1°; and at $T = 90$ sec, ϕ_{max} was reduced by about 17° and β_{max} was reduced by about 3°. It should be noted that when the $\delta_{sp} = 15°$ data are compared with data from base-line flow fields in ground effect (fig. 18) rather than with data out of ground effect, the initial responses are essentially the same. This indicates that at $T = 60$ sec and 90 sec, the attenuating effect of the ground plane and the attenuating effect of the 15° spoilers are essentially the same.

The fixed-controls data in figure 23(b) show that at $T = 45$ sec, the use of 30° spoilers reduced ϕ_{max} by about 7° and β_{max} by about 2°. These data also show that at $T = 60$ sec the initial upset with $\delta_{sp} = 30°$ was more severe than at $T = 45$ sec and that there was generally no spoiler-attenuation effect. This result is attributable to the previously noted anomaly in figure 8(b), where the values of V_{tan} at $T = 60$ sec are greater than at $T = 45$ sec.

The data in figure 23 for the piloted encounters show generally the same trends as the fixed-control data and also show lower values of ϕ_{max} and β_{max}. Figure 24 shows motion histories following piloted encounters both with the flow fields for $\delta_{sp} = 15°$ at $T = 90$ sec and with the base-line flow field out of ground effect at the same age. It can be seen that the magnitude of the Dutch roll oscillation was reduced with the $\delta_{sp} = 15°$ flow field because of the initial upset values of ϕ_{max} and β_{max}. Even with these reductions, however, the oscillation was still large and required about 15 sec to damp out.

ACCEPTABLE UPSETS

This section of the paper discusses two altitude-dependent criteria for acceptable upsets at low altitudes. The simulator results are then evaluated by comparison with the criteria.

Criteria for Acceptable Upsets

In the absence of completely defined criteria for acceptable vortex-induced upsets, this study utilized a combination of VFR bank-angle criteria from an earlier NASA investigation and flight-path deviation criteria from current IFR operating procedures. Although these criteria are not compatible, they did provide standards against which the results of the simulations could be evaluated.

An earlier simulator study at the Ames Research Center (ref. 11) defined a criterion for acceptable, vortex-induced bank angles. (This criterion was defined for the Boeing 707 airplane and the Gates Learjet airplane, and it was used in ref. 12 in the analysis of automatic landing systems.) Since the results of the study discussed herein indicated that flight-path changes were also significant, additional criteria were examined for flight-path excursions.

The bank-angle criterion of reference 11 for the Boeing 707 airplane in VFR conditions was used for this study and is shown in figure 25. Since the airplane simulated in this study was lighter and smaller than the 707, some relaxing of the criterion in figure 25 might be justified by noting that the criterion in reference 11 for the Gates Learjet airplane was less stringent than for the heavier and

larger 707 airplane. However, to provide additional conservatism, the criterion for the 707 airplane was used directly.

A flight-path deviation criterion used by one major airline for IFR operations specifies that a missed approach be initiated whenever the glide slope or localizer course deviation exceeds ±1 dot on the Course Deviation Indicator (CDI). Data from reference 13, which lists 1 dot CDI deviations in terms of vertical- and lateral-position errors, are plotted as a function of distance from the target touchdown point x_E in figure 26.

For the purposes of this study, the Middle Marker beacon shown in figure 26 at x_E = 1.10 km (3600 ft) defines the point along the glide slope where the Decision Height (h = 57.5 m in this analysis) is reached. Since an IFR approach may not be continued below this height (the airplane must then either continue the approach visually or go around), the missed IFR approach criterion in figure 26 was not directly applicable at x_E < 1.10 km (3600 ft) and extrapolations were necessary. The extrapolations, which are shown by the dashed lines in figure 26, were based on the low-altitude path-excursion limits of reference 14. These limits are used in the certification of Flight Directors for Category II approaches and require that, at h = 30.5 m, the vertical-path excursions shall not exceed 3.7 m and the lateral-path excursions shall not exceed 19.5 m. Therefore, the criteria were extrapolated from Δh = 4.6 m at the Middle Marker to Δh = 3.7 m at h = 30.5 m (x_E = 0.58 km), and also from Δy = 76.5 m at the Middle Marker to Δy = 19.5 m at x_E = 0.58 km as shown.

Evaluation of Data

When the bank angle and flight-path excursion results were compared with the criterion at h_e = 61.0 m and 30.5 m, it was found that the only encounters in which both criteria might be satisfied were for the mildest condition where the flow field was in ground effect at T = 120 sec. The separation interval equivalent to T = 120 sec was 8.65 km (4.67 n. mi.).

This flow field was selected for an additional study of acceptable upsets, and the results are shown in table IV. Piloted encounters, centered with both the right- and left-wing vortices, were made at h_e = 76.2 m (250 ft), h_e = 54.9 m (180 ft), and h_e = 30.5 m (100 ft). Maximum bank angles and flight-path excursions are noted in the table, along with the initial maximum rolling- and yawing-moment coefficients experienced in each encounter.

The vertical-path excursion data from table IV are plotted against the path criterion in figure 27. Similarly, figure 28 shows the bank-angle data from table IV plotted against that criterion. (In plotting fig. 28, the direction of the data was neglected and all data were plotted as positive.) Since an examination of the lateral-path deviations (Δy) in table IV shows that all of these values were well within acceptable values (see fig. 26(b)), these data were not plotted.

The data in figure 27 show that the vertical-path excursions were acceptable at x_E > 0.58 km (h_e > 30.5 m) where the criterion could be applied. The pilot's evaluation of the data at x_E < 0.58 km was that these excursions were also acceptable since they should not require a missed VFR approach. The bank-angle data in figure 28 show that, for the encounters at h_e = 30.5 m, the ϕ_{max} values were all unacceptable. At both h_e = 54.9 m and h_e = 76.2 m, however, about half of the

upsets were acceptable and the other half were unacceptable when using the 707 bank-angle criterion from figure 25.

The pilot's evaluation of the encounters listed in table IV was that, for the airplane simulated herein, the upsets at h_e = 76.2 m (250 ft) and 54.9 m (180 ft) were all acceptable since these bank angles and flight-path excursions would not require missed VFR approaches. However, the pilot evaluated all of the upsets at h_e = 30.5 m as unacceptable since (as a result of the vortex-induced bank angles) missed approaches appeared preferable to continued approaches from this altitude.

The data in figure 29 define the largest allowable value of $C_{l,max}$ to assure acceptable bank angles for the simulated airplane at all altitudes above the threshold crossing height. The data are from centered, piloted encounters with the base-line flow field in ground effect. The data at $C_{l,max}$ = 0.134, 0.119, and 0.083 are from figure 18 (at T = 45, 60, and 90 sec, respectively), and the data at $C_{l,max}$ = 0.040 and 0.034 are mean values from table IV for T = 120 sec. (In plotting fig. 29, all $C_{l,max}$ and ϕ_{max} data were again treated as positive.) The bank-angle criterion at the nominal threshold crossing height of 16 m is from figure 25.

Extrapolation of the ϕ_{max} data shown by the dashed line in figure 29 indicates that the vortex-induced bank angles of the simulated airplane would be acceptable at all altitudes above, and including, the threshold crossing height if $C_{l,max}$ did not exceed 0.017. This allowable value of $C_{l,max}$ is about a factor of two less than the values shown for the mildest upsets in table IV. It should be noted that the Federal Aviation Administration is evaluating the feasibility of using ground-based equipment to indicate when the approach path is free of vortex disturbances. (See ref. 15.) If such techniques prove feasible, the minimum acceptable criteria could be much less stringent than the threshold-crossing conditions shown in figure 29. For example, if it could be established that there were no vortices between the threshold and the Middle Marker (where h ≈ 57.5 m), the larger maximum bank-angle criteria at the higher altitude ($\phi_{max} \approx \pm 9°$) would apply and the corresponding value of $C_{l,max}$ would be about ±0.035.

REVIEW OF RESULTS

A simulator investigation of the response of a twin-engine, commercial, jet transport airplane to wake vortex encounters has been conducted. The simulations were performed with fixed controls and also with a pilot using a state-of-the-art, manual-control system. A vortex flow field, modeled for a heavy, four-engine, commercial, jet transport airplane in the normal-approach configuration, speed, and lift coefficient, was the base line for the investigation. The following airplane was subjected to the constant-strength vortex flow field for a longitudinal distance of 76.2 m.

Simulated, piloted encounters with the base-line flow field out of ground effect, at a vortex age of 120 sec, showed that the maximum initial bank angle decreased from -40° (for encounters centered with the right-wing vortex) to about -17° for lateral offsets of ±8 m. The maximum initial sideslip angle decreased from about -10° for centered encounters to about -5° for lateral offsets of ±8 m. Lateral offsets were found to produce significant pitching moments as well as significant lift losses in a vortex downwash field. Following all of the encounters with this flow field, the airplane experienced large and persistent Dutch roll oscillations which made the recovery maneuver difficult at an encounter altitude of 61 m. The

lift losses from the laterally offset locations which produced downwash resulted in high rates of descent in the vertical flight path following the encounters.

A study of the effect of the vertical location of the same base-line flow field showed that, for the piloted simulations, the maximum initial bank angle decreased from about -40° for encounters centered with the right-wing vortex to about -18° for vertical offsets of ±8 m. The maximum initial sideslip angle decreased from about -10° for centered encounters to about -4° for vertical offsets of ±8 m. Vertical offsets had little effect on the initial lift or pitching-moment coefficients, and the vertical-path changes were all less severe than for laterally offset flow-field locations. As in the case of the lateral offsets, however, large and persistent Dutch roll oscillations occurred during the recovery maneuver.

The effect of increasing flow-field age out of ground effect was found to decrease the initial maximum bank angle from -48° at an age of 45 sec to -40° at an age of 120 sec for the piloted simulations. The effect of vortex age on the maximum initial sideslip angle was quite small for this flow field. Large Dutch roll oscillations occurred following all of these encounters. The effect of increasing flow-field age in ground effect was very significant. For piloted encounters, this effect decreased the initial maximum bank angle from -42° at an age of 45 sec to -11° at an age of 120 sec. The maximum initial sideslip angle decreased from -11.5° to -3.2° between ages of 45 and 120 sec. The piloted encounters with the base-line flow field in ground effect at an age of 120 sec resulted in the smallest initial upsets and the most easily managed recoveries in the investigation.

Increasing the approach speed of the simulated airplane from a nominal value of 125 knots to a value of 140 knots showed that, in the piloted simulations, the severity of the initial upset was essentially unaffected by an increase in speed. There was some improvement in the recovery maneuver as a result of improved control effectiveness at increased speed. Even with this favorable effect, however, the time required to damp out the vortex-induced oscillation was unsatisfactorily long.

Decreasing the approach lift coefficient of the generating airplane resulted in significantly less severe initial upsets when the following airplane encountered the flow field with fixed controls. Increasing the approach lift coefficient had the opposite effect.

When the flight spoilers of the generating airplane were deflected 15° as vortex attenuators, it was found that the severity of the initial upset with fixed controls was generally less than from comparable encounters with the base-line flow field out of ground effect. At a vortex age of 60 sec the maximum initial bank angle was reduced by about 10°, and at 90 sec the corresponding reduction was about 17°. The magnitude and duration of the body motions following the encounter were also reduced by the 15° spoiler deflection, although the recovery was still considered to be difficult.

For this study, altitude-dependent criteria were used to define acceptable vortex-induced bank angles and flight-path excursions for the simulated airplane. None of the initial upsets from encounters with the base-line flow field out of ground effect were acceptable either with fixed controls or with the pilot using the manual-control system. Some acceptable upsets were observed following piloted encounters with the base-line flow field in ground effect at an age of 120 sec. None of these upsets were acceptable, however, at the lowest encounter altitude of 30.5 m because of excessive bank-angle excursions.

Langley Research Center
National Aeronautics and Space Administration
Hampton, VA 23665
December 18, 1981

APPENDIX

CALCULATIONS OF VORTEX-INDUCED FORCES AND MOMENTS

This appendix is included to present additional details on the method of calculating the forces and moments imposed on the simulated airplane by the vortex segment. Summary discussions of the strip geometry, computation sequence, and the force and moment equations are included. Additional details on the general method are presented in reference 7.

Vortex-induced forces and moments on the wing and tail surfaces were calculated by using strip theory. In this study, the wing was divided into 36 chordwise strips of equal width along the span, and the horizontal tail was divided into 12 chordwise strips of equal width along the span. The vertical tail was divided into six chordwise strips of equal height. The incremental force on each of these strips was assumed to act at a reference point located at the intersection of the $0.25\bar{c}$ point and the center line of each strip. Vortex effects on the fuselage were calculated as pitching and yawing moments proportional to the induced angles of attack and sideslip at the c.g.

In a typical computation, the locations and orientations of both the simulated airplane and the flow field were established with respect to an Earth-fixed reference system (X_E, Y_E, Z_E) as shown in figure 9. The locations of the reference points on the airplane were then determined relative to the centers of both vortices, and $(V_{tan})_{Y_E}$ and $(V_{tan})_{Z_E}$ were calculated at each reference point by using equations (1) and (2).

The vortex-imposed velocity increments and the airplane velocity and attitude data were then used to calculate the vortex-induced $\Delta\alpha$ and $\Delta\beta$ at each reference point. These data were then used to calculate the vortex forces and moments on the strips (in the X_B, Y_B, and Z_B body-axis system shown in fig. 9). Total forces and moments were summations of the strip values. The equations used for calculating the total, vortex-induced forces and moments were as follows:

$$F_{X,t} = F_{X,w} + F_{X,h} \tag{A1}$$

$$F_{Y,t} = F_{Y,v} \tag{A2}$$

$$F_{Z,t} = F_{Z,w} + F_{Z,h} \tag{A3}$$

$$M_{X,t} = M_{X,w} + M_{X,h} + M_{X,v} \tag{A4}$$

$$M_{Y,t} = M_{Y,w} + M_{Y,h} + M_{Y,F} \tag{A5}$$

$$M_{Z,t} = M_{Z,w} + M_{Z,h} + M_{Z,v} + M_{Z,F} \tag{A6}$$

These vortex-induced forces and moments were then added to the other forces and moments acting on the simulated airplane during passage through the vortex segment.

The unsymmetrical $\Delta\alpha$ imposed on the wing and horizontal tail by the vortex produced longitudinal and vertical body-axis forces which were calculated as follows:

$$F_{X,w} = -\bar{q}\left[\sum_{1}^{36} S_{i,w}\left(C_{D,i,w}\cos\alpha - C_{L,i,w}\sin\alpha\right)\right] \tag{A7}$$

$$F_{X,h} = -\bar{q}\left[\sum_{1}^{12} S_{i,h}\left(C_{L,i,h}\sin\alpha\right)\right] \tag{A8}$$

$$F_{Z,w} = -\bar{q}\left[\sum_{1}^{36} S_{i,w}\left(C_{L,i,w}\cos\alpha + C_{D,i,w}\sin\alpha\right)\right] \tag{A9}$$

$$F_{Z,h} = -\bar{q}\left[\sum_{1}^{12} S_{i,h}\left(C_{L,i,h}\cos\alpha\right)\right] \tag{A10}$$

In these equations, $C_{L,i}$ and $C_{D,i}$ are the strip lift and drag coefficients which are functions of $\Delta\alpha_i$.

Vortex-imposed crossflow on the vertical tail resulted in a side force given by

$$F_{Y,v} = \bar{q}\left(\sum_{1}^{6} S_{i,v}C_{Y_{\beta,v}}\Delta\beta_i\right) \tag{A11}$$

The rolling moments of the wing, horizontal tail, and vertical tail were determined from

$$M_{X,w} = \sum_{1}^{36} F_{Z,i,w}y_{B,i,w} \tag{A12}$$

$$M_{X,h} = \sum_{1}^{12} F_{Z,i,h} y_{B,i,h} \tag{A13}$$

$$M_{X,v} = \sum_{1}^{6} -F_{Y,i,v} z_{B,i,v} \tag{A14}$$

The pitching moments of the wing and horizontal tail were

$$M_{Y,w} = \sum_{1}^{36} -F_{X,i,w} z_{B,i,w} + \sum_{1}^{36} -F_{Z,i,w} x_{B,i,w} \tag{A15}$$

$$M_{Y,h} = \sum_{1}^{12} -F_{X,i,h} z_{B,i,h} + \sum_{1}^{12} -F_{Z,i,h} x_{B,i,h} \tag{A16}$$

and the yawing moments of the wing, horizontal tail, and vertical tail were, respectively,

$$M_{Z,w} = \sum_{1}^{36} -F_{X,i,w} y_{B,i,w} \tag{A17}$$

$$M_{Z,h} = \sum_{1}^{12} -F_{X,i,h} y_{B,i,h} \tag{A18}$$

$$M_{Z,v} = \sum_{1}^{6} F_{Y,i,v} x_{B,i,v} \tag{A19}$$

As in reference 7, the vortex-induced fuselage pitching and yawing moments were

$$M_{Y,F} = M_{Y_{\alpha,F}} \Delta\alpha_F \tag{A20}$$

$$M_{Z,F} = M_{Z_{\beta,F}} \Delta\beta_F \tag{A21}$$

In equations (A20) and (A21) the airplane c.g. was the fuselage reference point for the calculation of $\Delta\alpha_F$ and $\Delta\beta_F$. The aerodynamic data required by the preceding equations were determined primarily from the wind-tunnel tests described in reference 6.

REFERENCES

1. Hastings, Earl C., Jr.; Holdbrook, G. Thomas; and Keyser, Gerald L., Jr.: Preliminary Results of Simulated Vortex Encounters by a Twin-Engine, Commercial Aircraft During Final Landing Approach. NASA TM-81782, 1980.

2. Hastings, Earl C., Jr.; and Keyser, Gerald L., Jr.: Simulated Vortex Encounters by a Twin-Engine Commercial Transport Aircraft During Final Approach. [Preprint] 800775, Soc. Automot. Eng., May 1980.

3. Parrish, Russell V.; Dieudonne, James E.; Martin, Dennis J., Jr.; and Copeland, James L.: Compensation Based on Linearized Analysis for a Six-Degree-of-Freedom Motion Simulator. NASA TN D-7349, 1973.

4. Dieudonne, James E.: Description of a Computer Program and Numerical Technique for Developing Linear Perturbation Models From Nonlinear Systems Simulations. NASA TM-78710, 1978.

5. Parrish, Russell V.; Kahlbaum, William M., Jr.; and Steinmetz, George G.: Effect of Image Tilt of a Virtual Image Display on Simulated Transport Touchdown Performance. NASA TP-1520, 1979.

6. Paulson, John W., Jr.: Wind-Tunnel Results of the Aerodynamic Characteristics of a 1/8-Scale Model of a Twin-Engine Short-Haul Transport. NASA TM X-74011, 1977.

7. Johnson, Walter A.; and Teper, Gary L.: Analysis of Vortex Wake Encounter Upsets. NASA CR-127491, 1974.

8. Ciffone, Donald L.; and Pedley, Barbara: Measured Wake-Vortex Characteristics of Aircraft in Ground Effect. J. Aircr., vol. 16, no. 2, Feb. 1979, pp. 102-109.

9. Nguyen, Luat T.; Ogburn, Marilyn E.; Gilbert, William P.; Kibler, Kemper S.; Brown, Phillip W.; and Deal, Perry L.: Simulator Study of Stall/Post-Stall Characteristics of a Fighter Airplane With Relaxed Longitudinal Static Stability. NASA TP-1538, 1979.

10. Croom, Delwin R.: Low-Speed Wing-Tunnel Parametric Investigation of Flight Spoilers as Trailing-Vortex-Alleviation Devices on a Transport Aircraft Model. NASA TP-1419, 1979.

11. Sammonds, Robert I.; Steinnett, Glen W., Jr.; and Larson, William E.: Criteria Relating Wake Vortex Encounter Hazard to Aircraft Response. J. Aircr., vol. 14, no. 10, Oct. 1977, pp. 981-987.

12. Tinling, Bruce E.: Estimates of the Effectiveness of Automatic Control in Alleviating Wake Vortex Induced Roll Excursions. NASA TM-73267, 1977.

13. Instrument Flying. AF Manual 51-37, Dept. Air Force, Dec. 1, 1976.

14. Criteria for Approving Category I and Category II Landing Minima for FAR 121 Operators. AC No. 120-29, FAA, Sept. 25, 1970.

15. Wood, William D., ed.: FAA/NASA Proceedings Workshop on Wake Vortex Alleviation and Avoidance. Rep. No. FAA-RD-79-105, Oct 1979. (Available from DTIC as AD A077 897 and from NASA as NASA CR-163317.)

TABLE I.- CHARACTERISTICS OF THE 737-100 AIRPLANE

SIMULATED IN THE INVESTIGATION

Wing dimensions:	
Area, m^2 (ft^2)	91.0 (980.0)
Span, m (ft)	28.3 (93.0)
Mean aerodynamic chord, m (ft)	3.4 (11.2)
Incidence angle, deg	1.0
Aspect ratio	8.83
Dihedral, deg	6.0
Sweep of quarter-chord, deg	25.0
Flap area, m^2 (ft^2)	14.9 (160.8)
Horizontal-tail dimensions:	
Area, m^2 (ft^2)	29.0 (312.0)
Span, m (ft)	11.0 (36.0)
Vertical-tail dimensions (exposed):	
Area, m^2 (ft^2)	20.8 (223.4)
Span, m (ft)	6.2 (20.2)
Fuselage dimensions:	
Length, m (ft)	27.6 (90.7)
Maximum diameter, m (ft)	4.0 (13.2)
Mass and inertia characteristics:	
Mass, kg (lb)	38 555 (85 000)
Center of gravity (percent $\bar{c}$)	19.0
Inertias, kg-m^2 (slug-ft^2):	
Roll	549 108 (405 000)
Pitch	1 080 591 (797 000)
Yaw	1 710 371 (1 261 500)

TABLE II.- VORTEX CONDITIONS MODELED IN THE INVESTIGATION

Vortex condition modeled	Configuration of generating airplane	Vortex ages modeled, sec
Base line, out of ground effect	Landing approach	45, 60, 90, 120
Base line, in ground effect	Landing approach	45, 60, 90, 120
High $C_{L,g}$	Landing approach	45, 60, 90, 120
Low $C_{L,g}$	Landing approach	45, 60, 90, 120
Attenuated (15° spoilers)	Landing approach with spoilers 2, 3, and 4 at 15°	60, 90
Attenuated (30° spoilers)	Landing approach with spoilers 2, 3, and 4 at 30°	45, 60

TABLE III.- TEST-CONDITION MATRIX

Effect studied	Velocity distribution	y_{vor}		z_{vor}		$C_{L,g}$	$C_{L,f}$	V_g, knots	V_f, knots	m_g	
		m	ft	m	ft					kg	lb
Lateral location	Fig. 5(a); T = 120 sec	9.14 4.57 0 -4.57 -9.14	30 15 0 -15 -30	$z_{vor} = 0$		1.40	1.62	140	125	231 293	509 914
Vertical location	Fig. 5(a); T = 120 sec	$y_{vor} = 0$		9.14 4.57 0 -4.57 -9.14	30 15 0 -15 -30	1.40	1.62	140	125	231 293	509 914
Vortex age out of ground effect	Fig. 5(a); T = 45, 60, 90, and 120 sec	Centered $y_{vor} = z_{vor} = 0$				1.40	1.62	140	125	231 293	509 914
Vortex age in ground effect	Fig. 5(b); T = 45, 60, 90, and 120 sec	Centered $y_{vor} = z_{vor} = 0$				1.40	1.62	140	125	231 293	509 914
Effect of V_f	Fig. 5(a); T = 120 sec	Centered $y_{vor} = z_{vor} = 0$				1.40	1.30	140	140	231 293	509 914
Effect of $C_{L,g}$	Figs. 6 and 7; T = 120 sec	Centered $y_{vor} = z_{vor} = 0$				1.54 and 0.98	1.62	140	125	255 826 and 161 978	564 000 and 357 100
Spoilers at 15° deflection	Fig. 8(a); T = 60 and 90 sec	Centered $y_{vor} = z_{vor} = 0$				1.40	1.62	140	125	231 293	509 914
Spoilers at 30° deflection	Fig. 8(b); T = 45 and 60 sec	Centered $y_{vor} = z_{vor} = 0$				1.40	1.62	140	125	231 293	509 914

TABLE IV.- INITIAL UPSET CHARACTERISTICS

[Centered, piloted encounters; base-line flow field in ground effect; T = 120 sec]

Right- or left-wing vortex	$C_{l,max}$	ϕ_{max}, deg	$C_{n,max}$	Δh, m	Δy, m
h_e = 76.2 m (250 ft)					
R	-0.0421	-12.7	0.0096	3.05	4.88
L	.0402	10.9	-.0084	1.22	2.74
R	-.0399	-11.2	.0089	2.44	3.65
L	.0406	10.8	-.0091	2.13	3.05
R	-.0388	-11.5	.0084	2.29	2.44
L	.0402	12.0	-.0085	3.05	2.74
h_e = 54.9 m (180 ft)					
L	0.0326	9.7	-0.0085	0.76	2.74
R	-.0322	-10.7	.0081	1.52	2.44
L	.0362	8.7	-.0088	2.29	0
h_e = 30.5 m (100 ft)					
R	-0.0366	-11.9	0.0089	1.52	3.05
L	.0353	8.7	-.0089	.61	2.74
R	-.0412	-10.6	.0093	1.83	4.27
R	-.0400	-10.9	.0081	.91	1.52
R	-.0386	-10.7	.0078	.91	2.44
R	-.0405	-11.4	.0081	.91	2.74
R	-.0439	-11.0	.0087	2.13	2.44
R	-.0443	-13.2	.0089	2.13	2.44
R	-.0390	-10.8	.0087	.91	3.05
R	-.0381	-9.2	.0089	1.22	1.83

L-74-5843

Figure 1.- Photograph of the Langley Visual/Motion Simulator.

L-75-7496

Figure 2.- Photograph of the visual landing display system at the Langley Research Center.

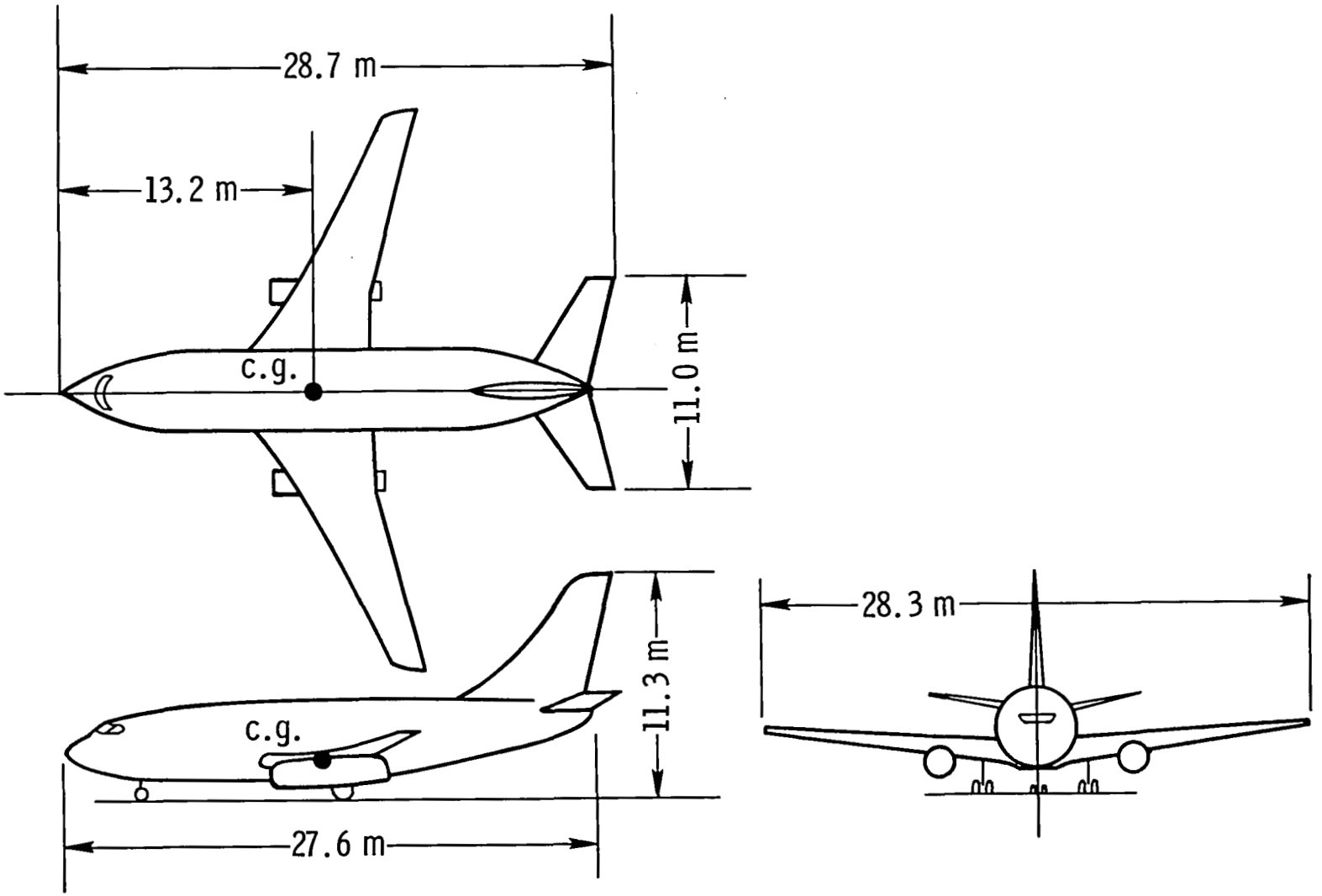

Figure 3.- Sketch of the 737-100 airplane simulated in this investigation.

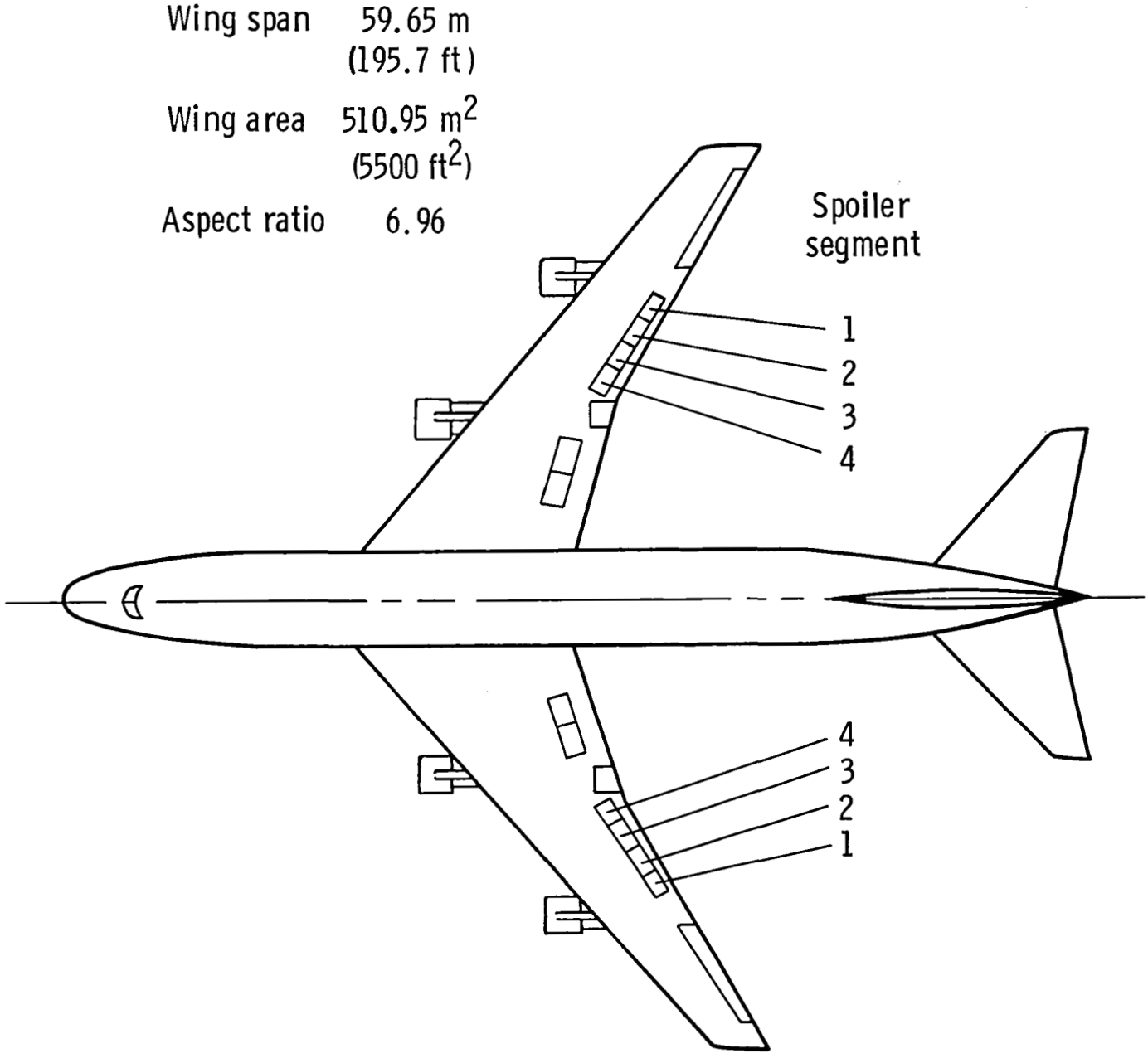

Figure 4.- Drawing of the vortex-generating airplane used in this investigation.

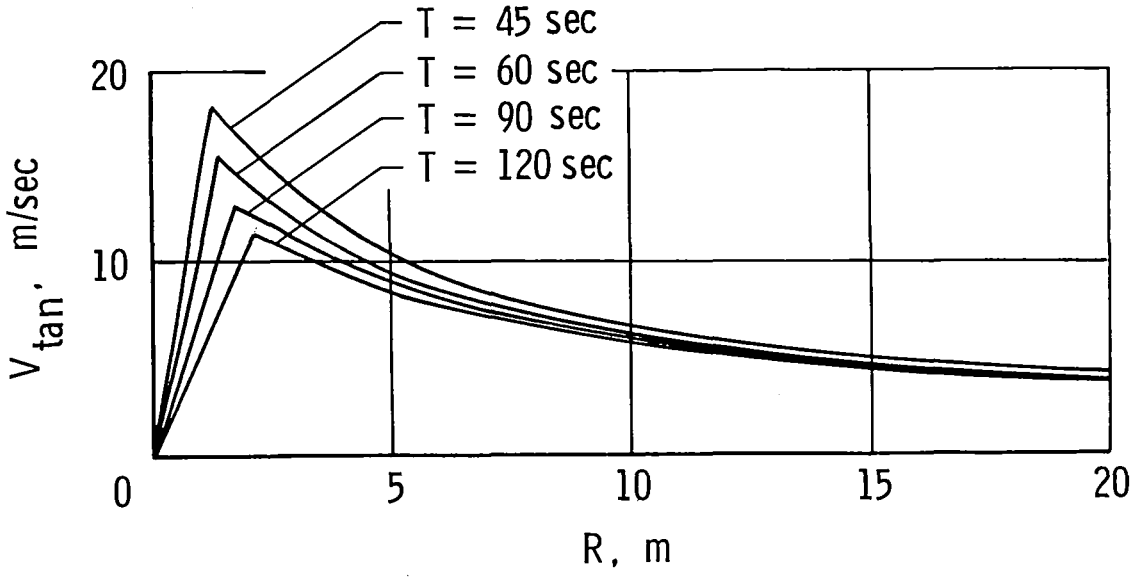

(a) Base-line vortex out of ground effect.

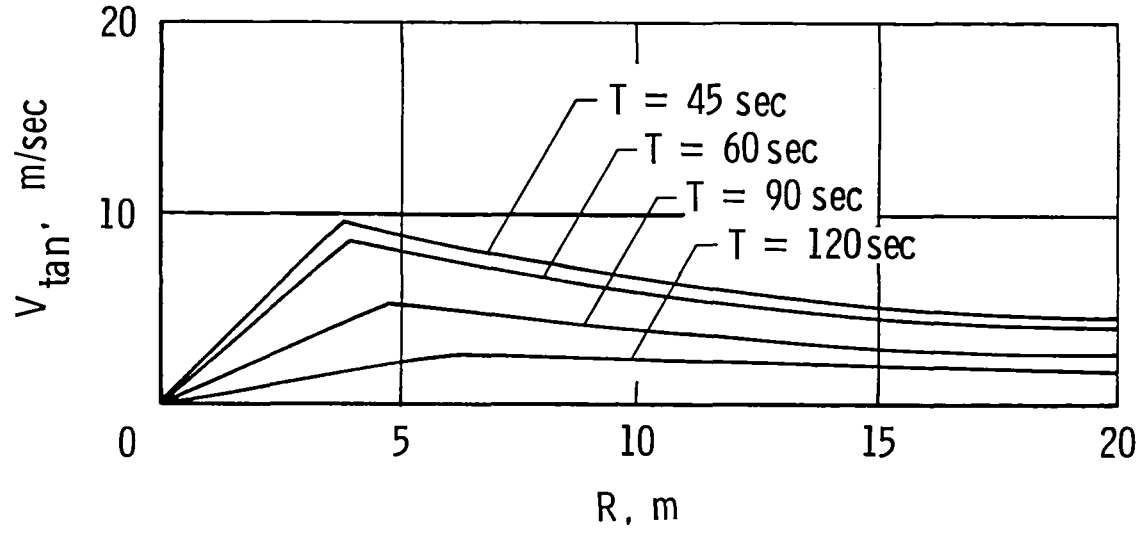

(b) Base-line vortex in ground effect.

Figure 5.- Base-line vortex velocity distributions.

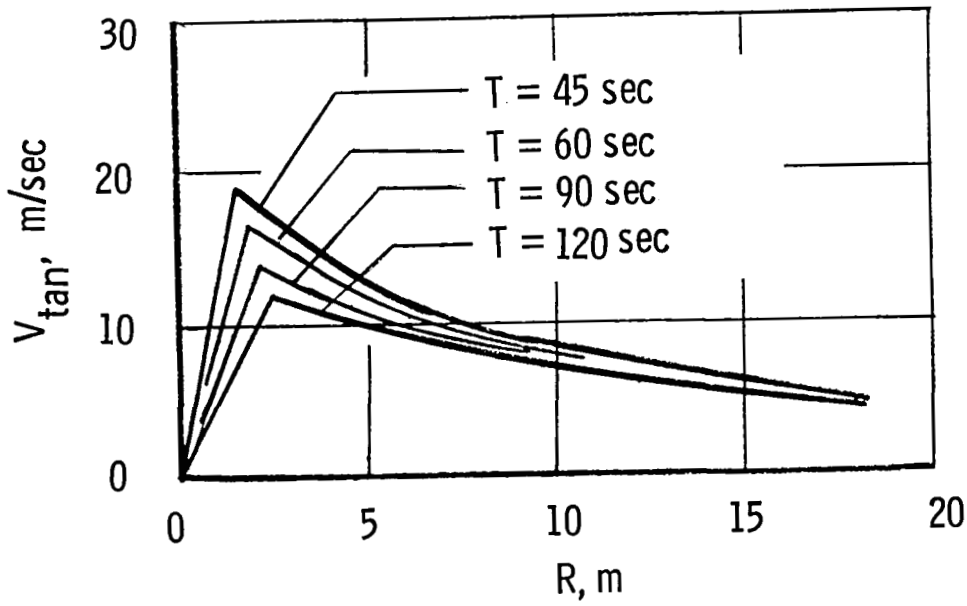

Figure 6.- Velocity distributions for high $C_{L,g}$ condition. $C_{L,g}$ = 1.54; V_g = 140 knots; vortex out of ground effect.

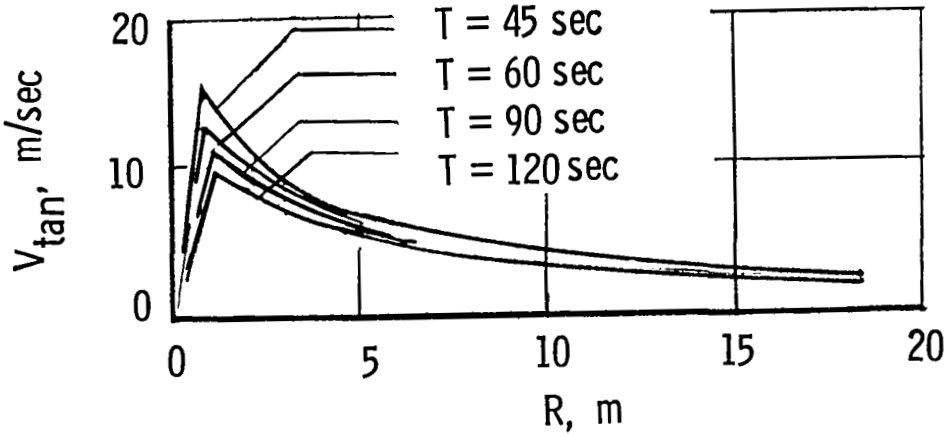

Figure 7.- Velocity distributions for low $C_{L,g}$ condition. $C_{L,g}$ = 0.98; V_g = 140 knots; vortex out of ground effect.

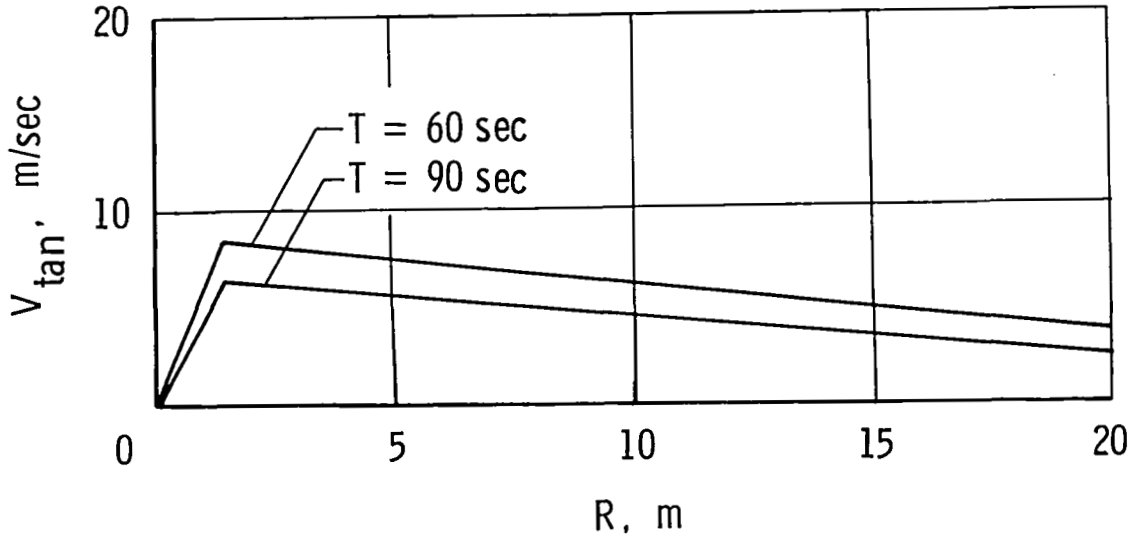

(a) Attenuated (15° spoilers).

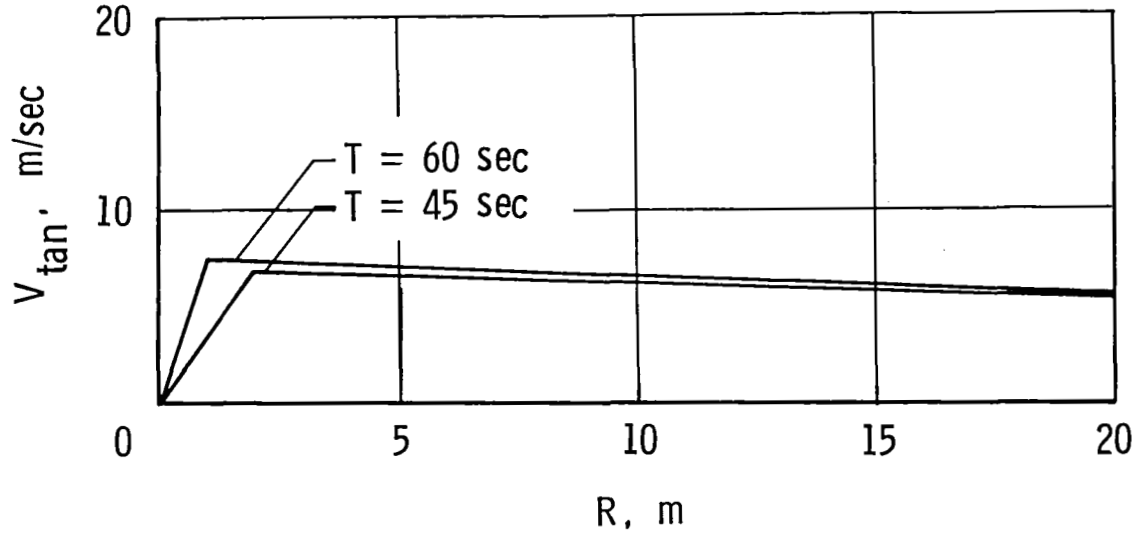

(b) Attenuated (30° spoilers).

Figure 8.- Vortex velocity distributions with spoilers deflected.

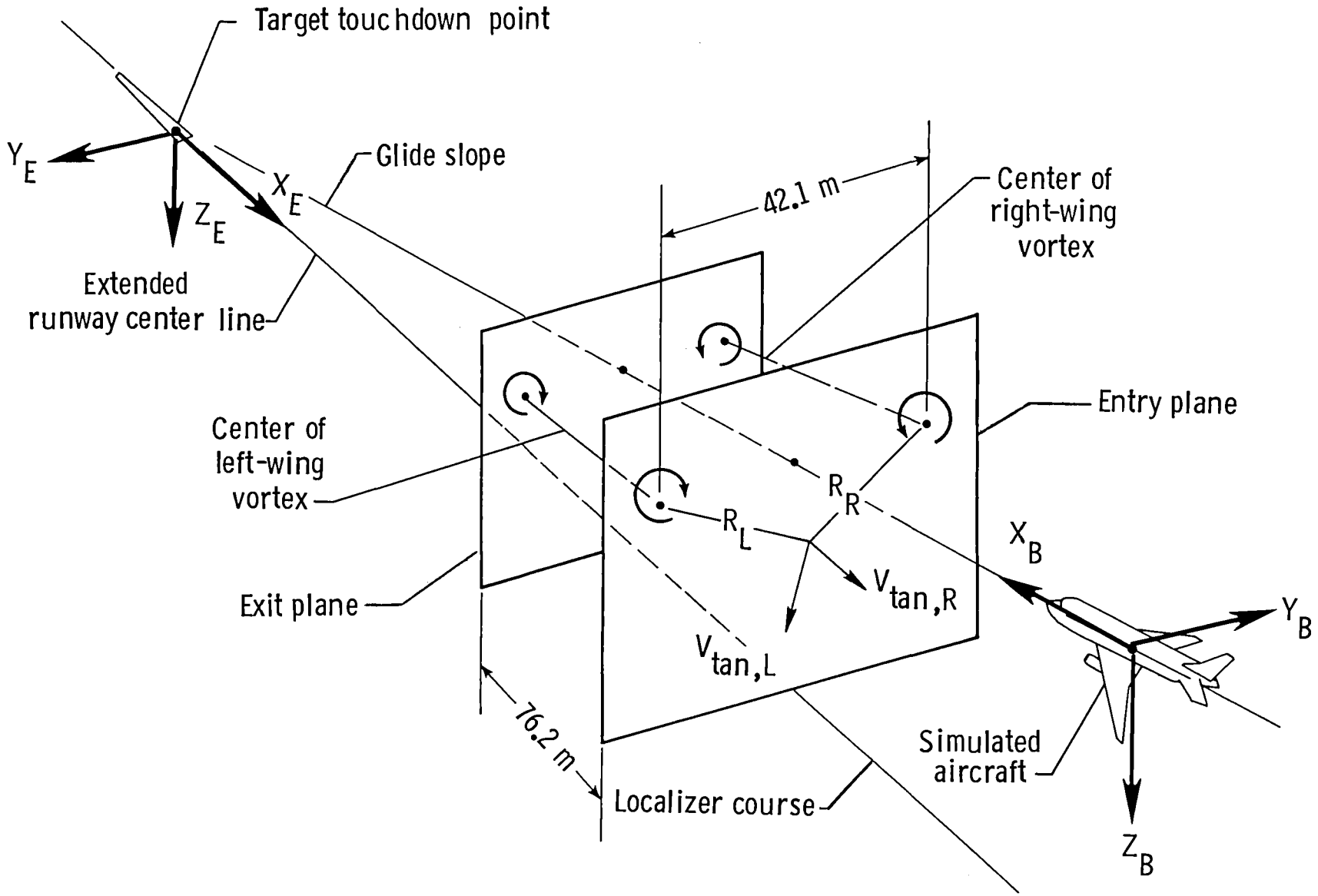

Figure 9.- Three-dimensional flow-field geometry.

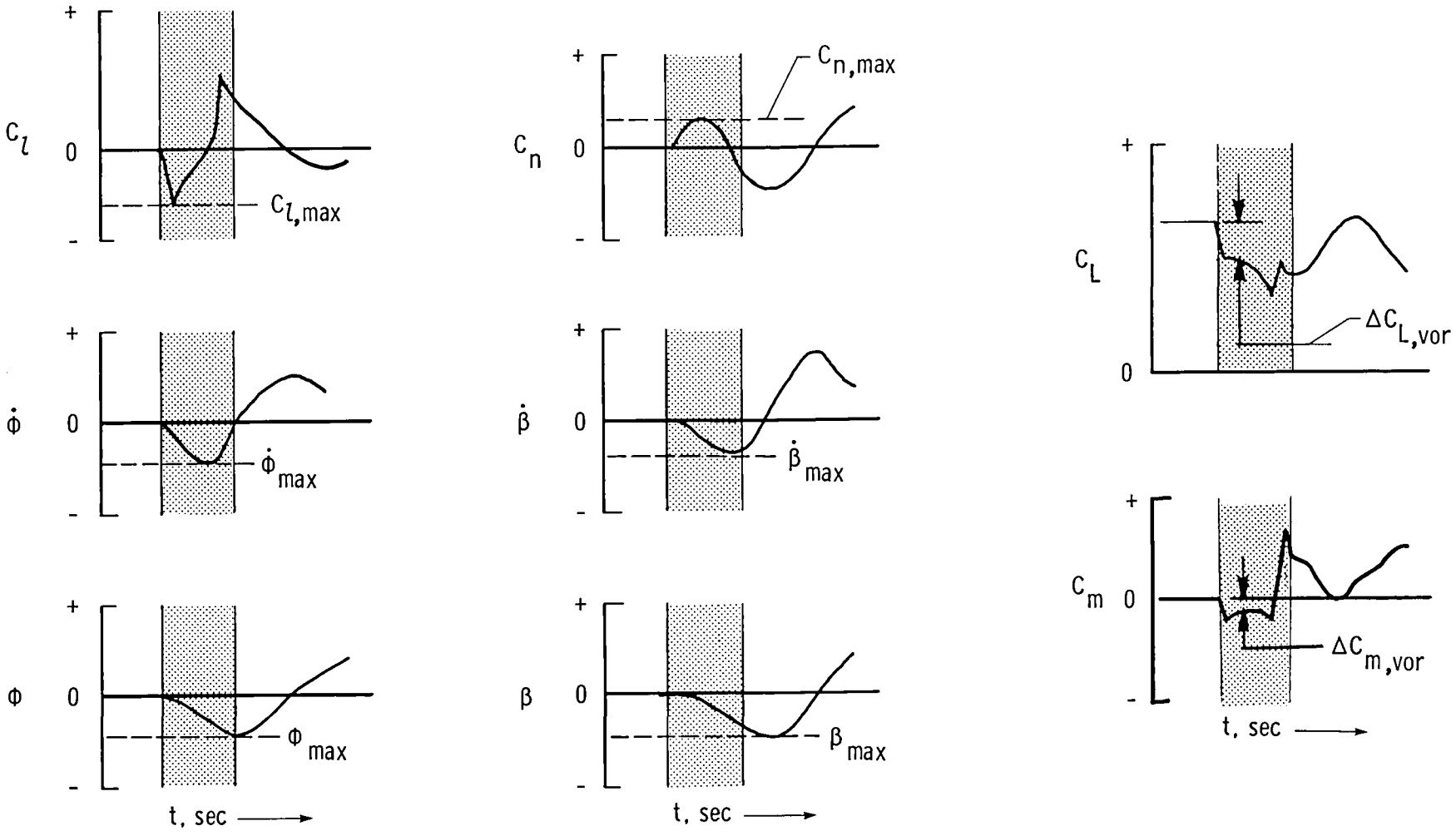

Figure 10.- Typical time histories illustrating data-analysis method. Shaded bands indicate time that simulated airplane is in the vortex segment.

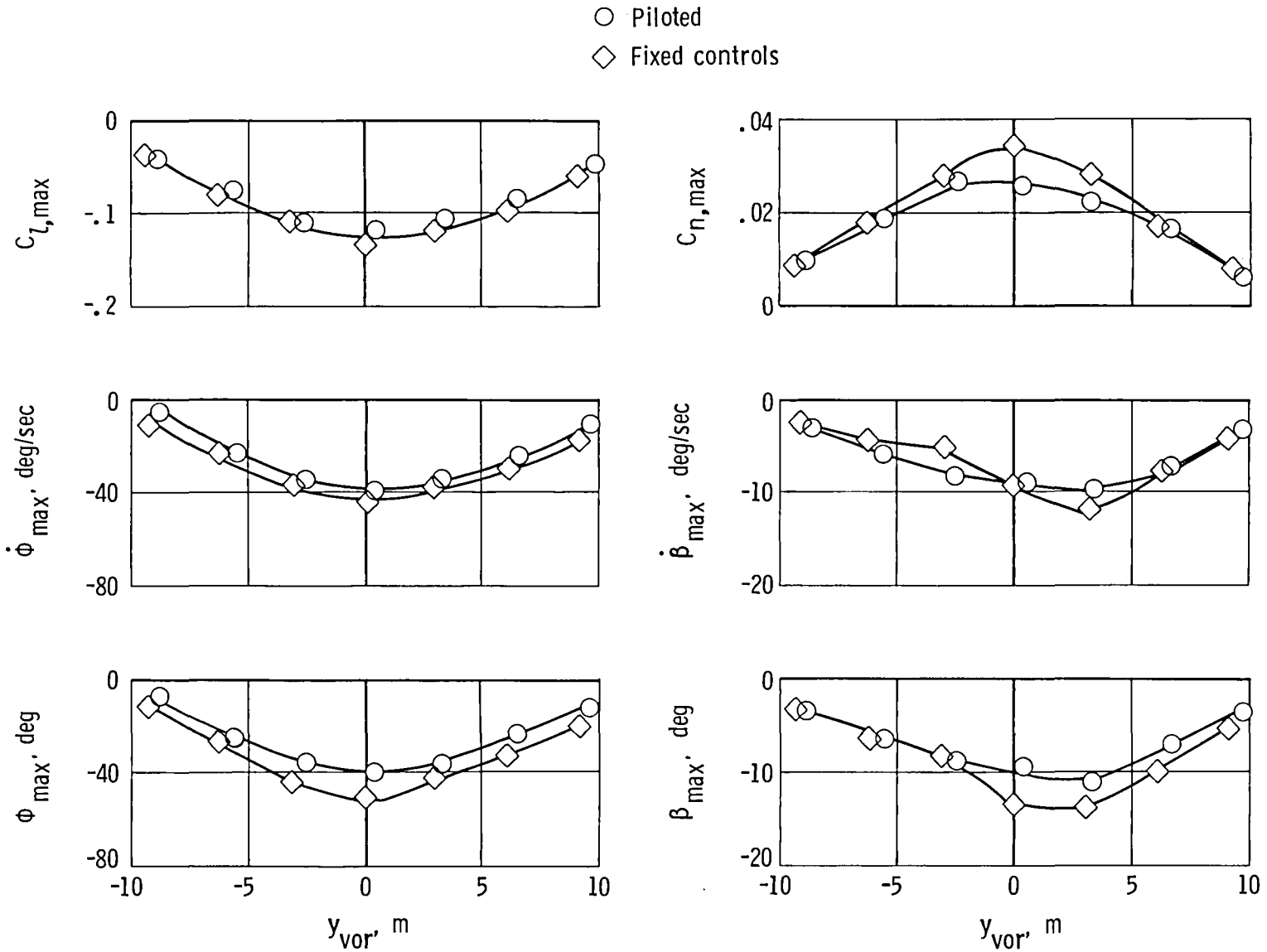

(a) Lateral-directional response.

Figure 11.- Effect of lateral location of vortex on initial response. Base-line vortex out of ground effect; T = 120 sec.

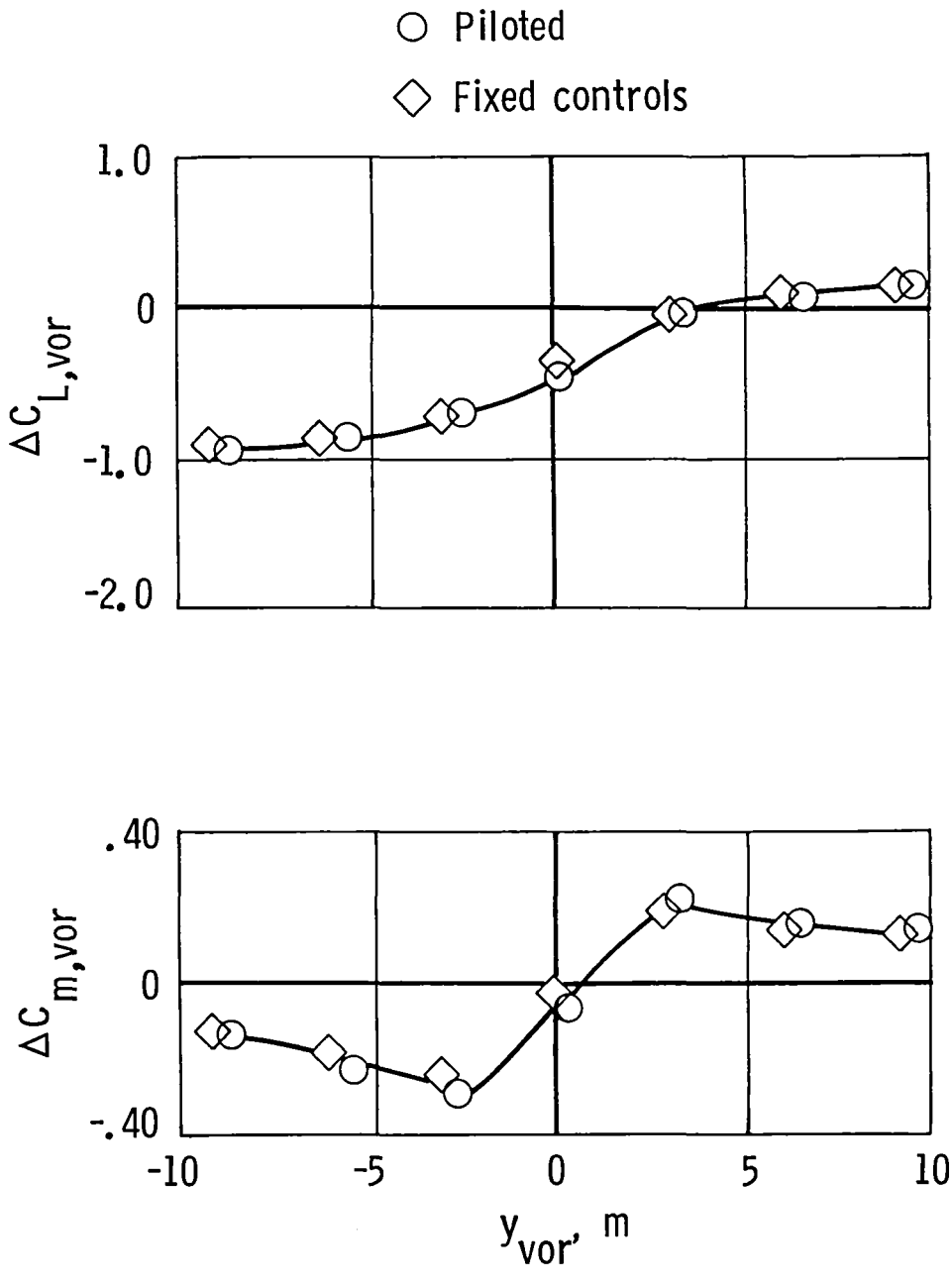

(b) Longitudinal response.

Figure 11.- Concluded.

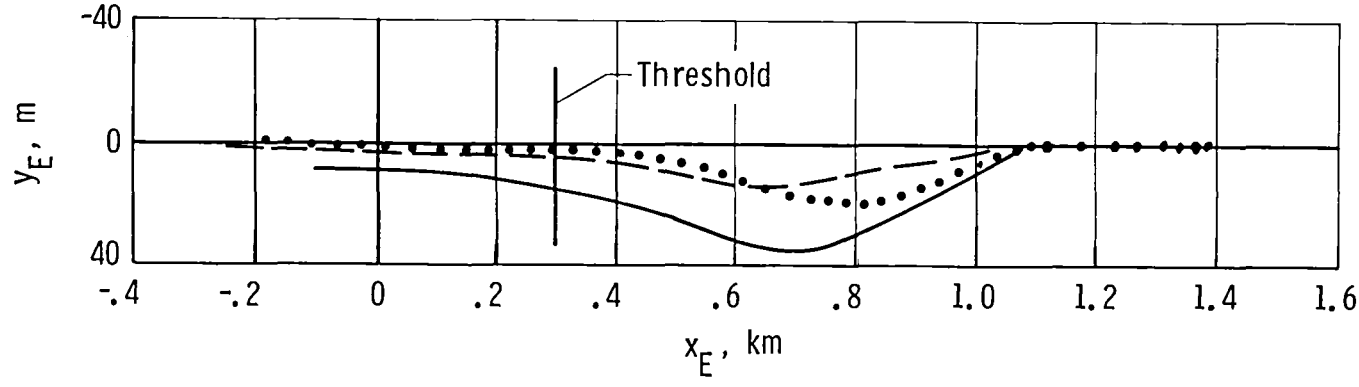

(a) Horizontal projection.

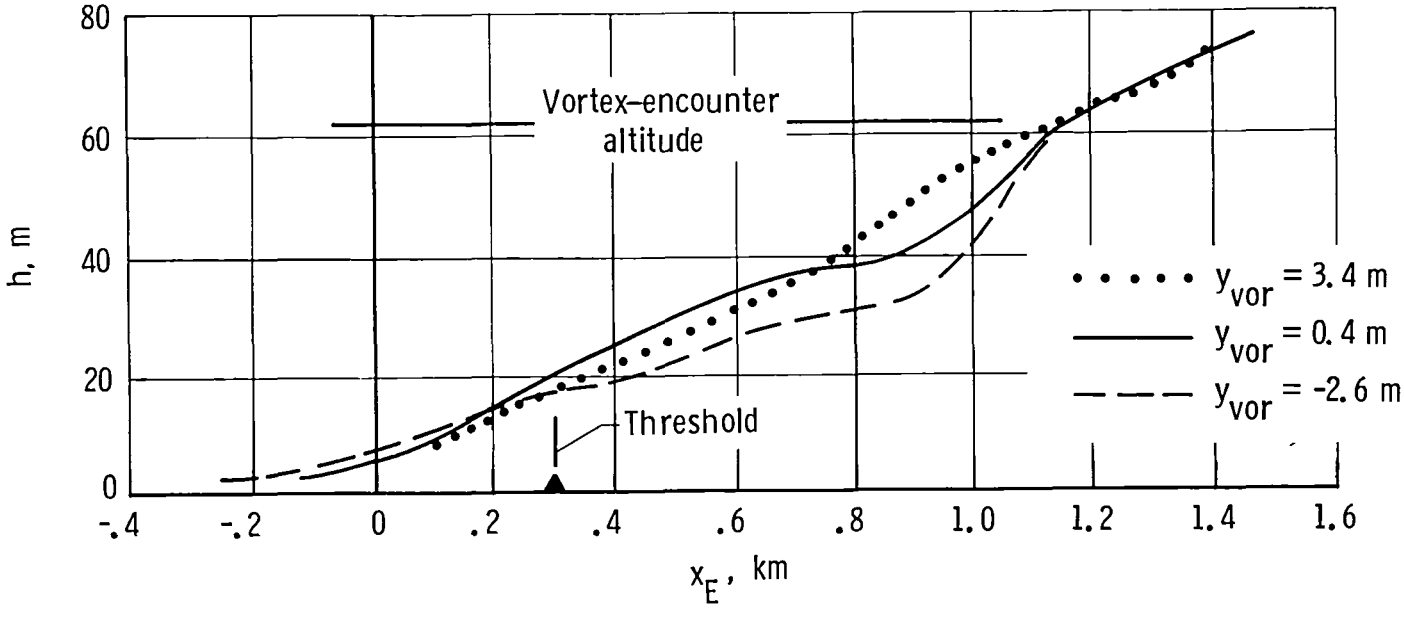

(b) Vertical projection.

Figure 12.- Effect of lateral location of vortex on flight path. Base-line vortex out of ground effect; T = 120 sec.

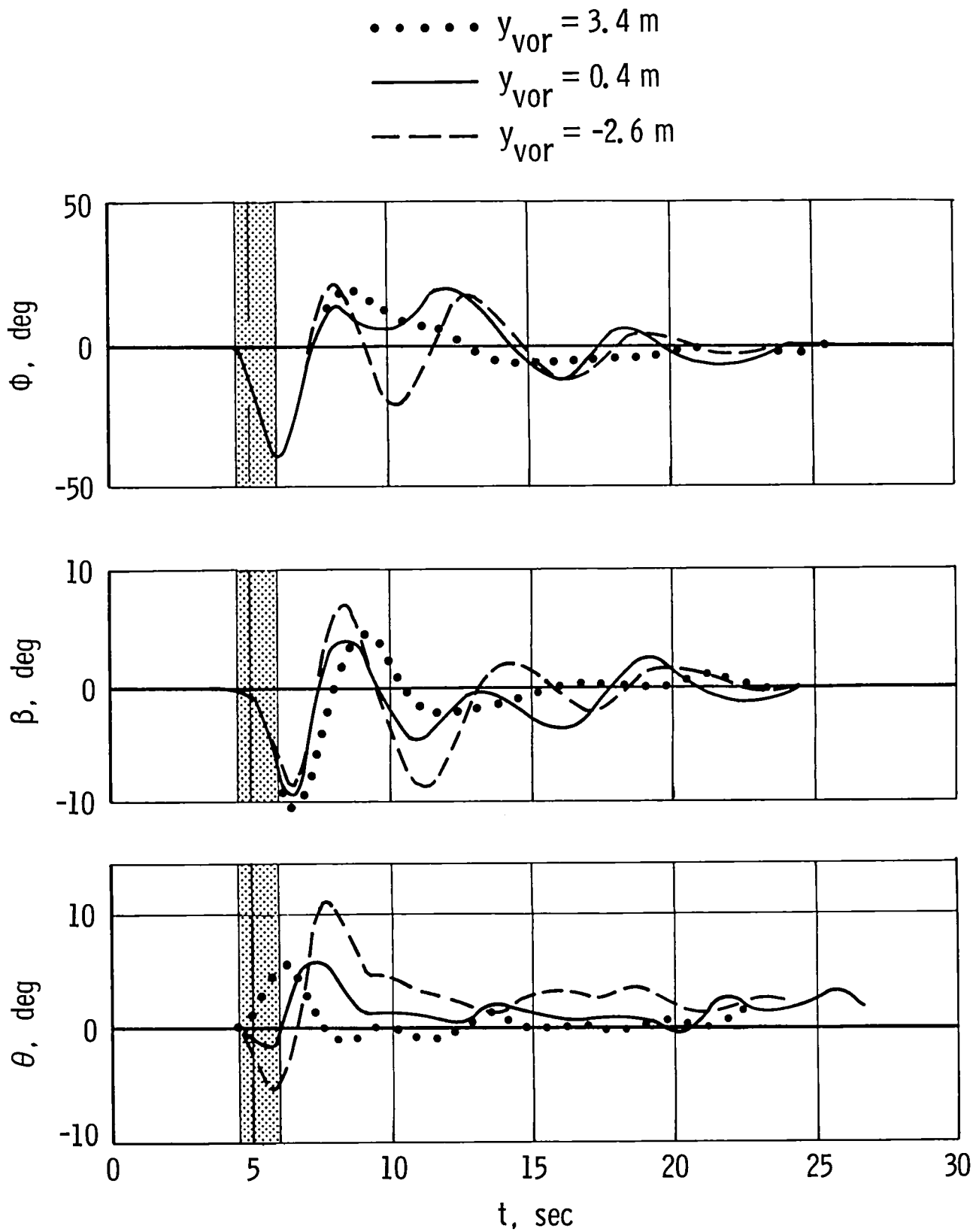

Figure 13.- Body attitudes following piloted encounters with a laterally displaced vortex. Base-line vortex out of ground effect; T = 120 sec.

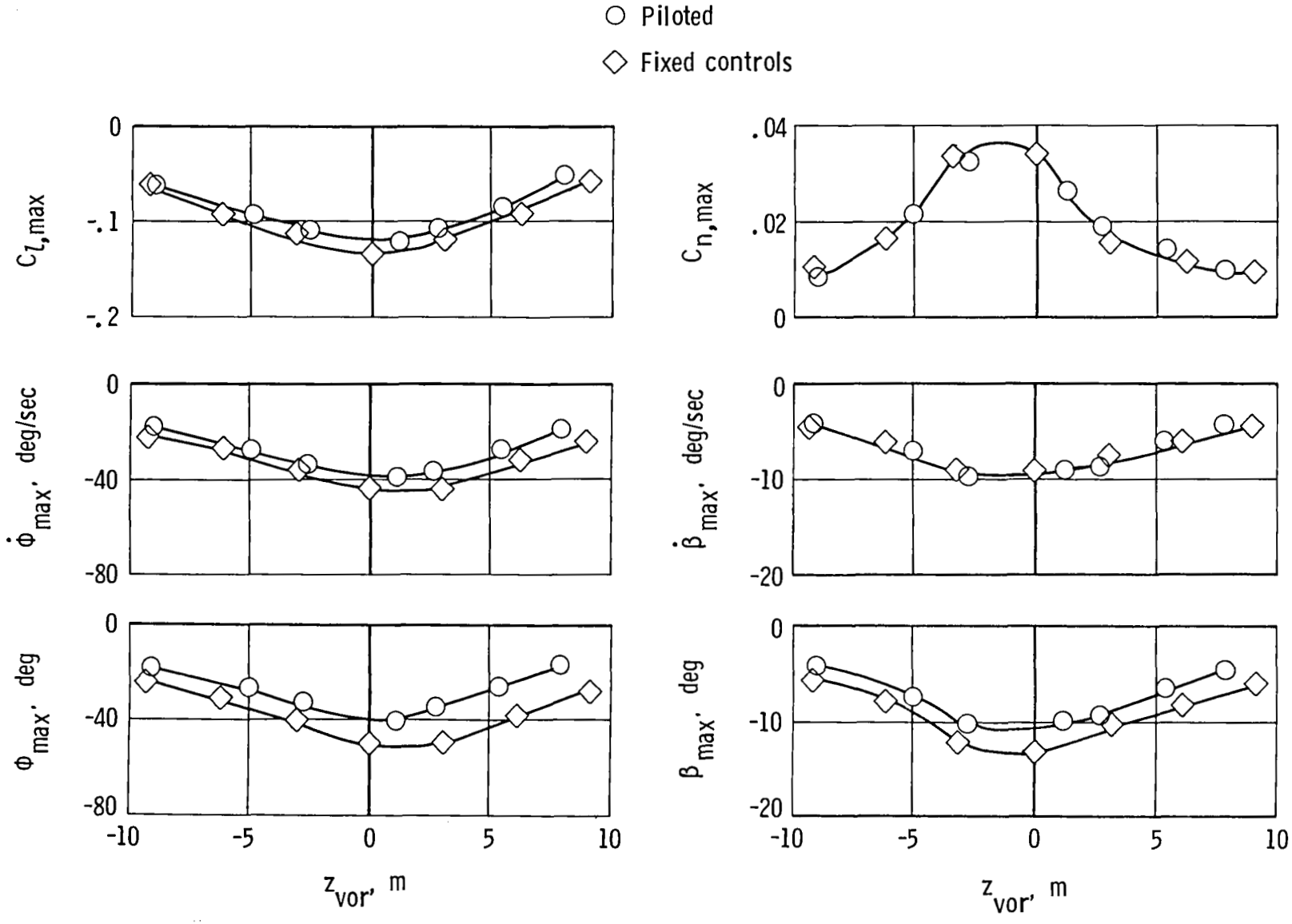

(a) Lateral-directional response.

Figure 14.- Effect of vertical location of vortex on initial response. Base-line vortex out of ground effect; T = 120 sec.

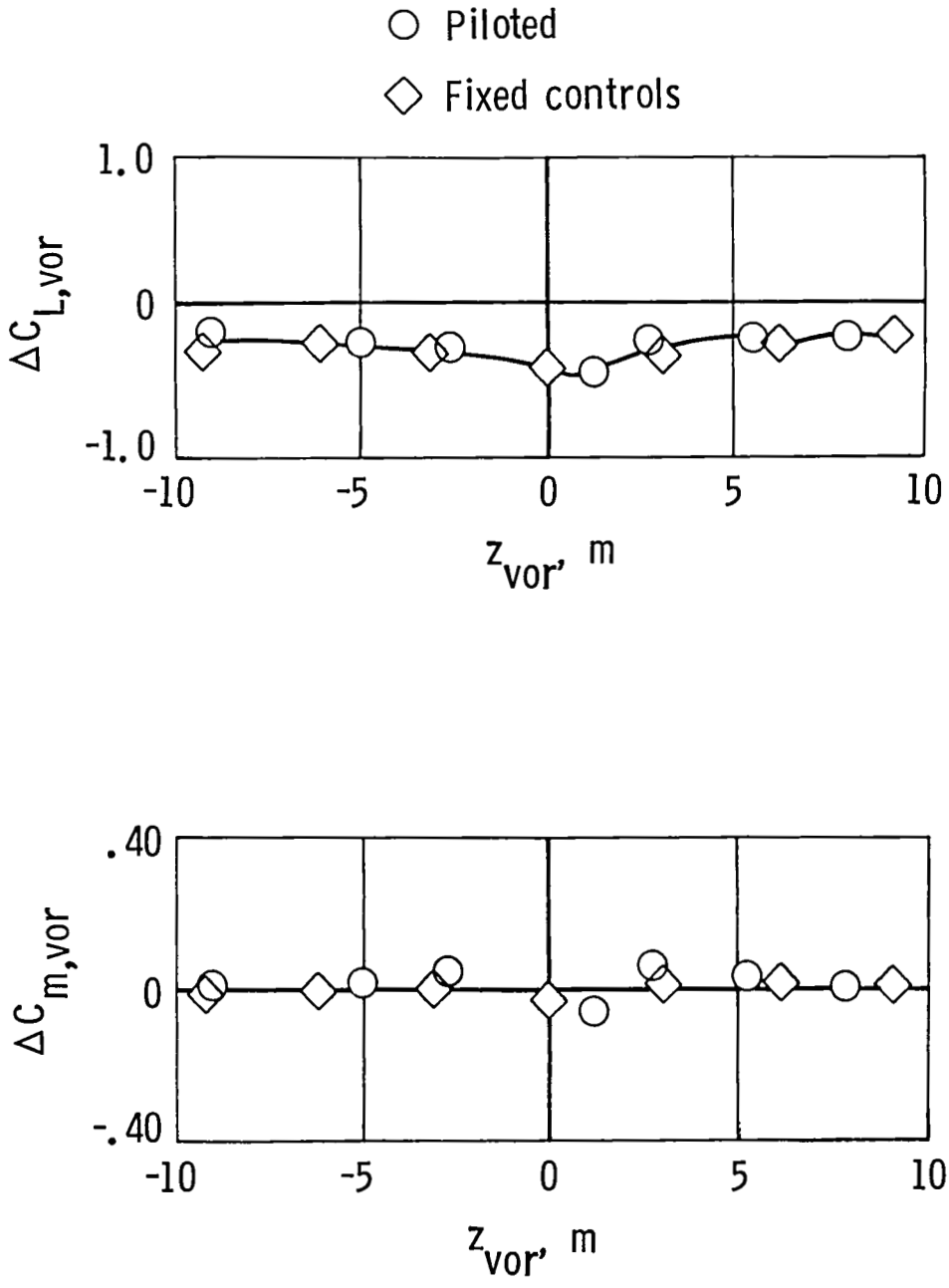

(b) Longitudinal response.

Figure 14.- Concluded.

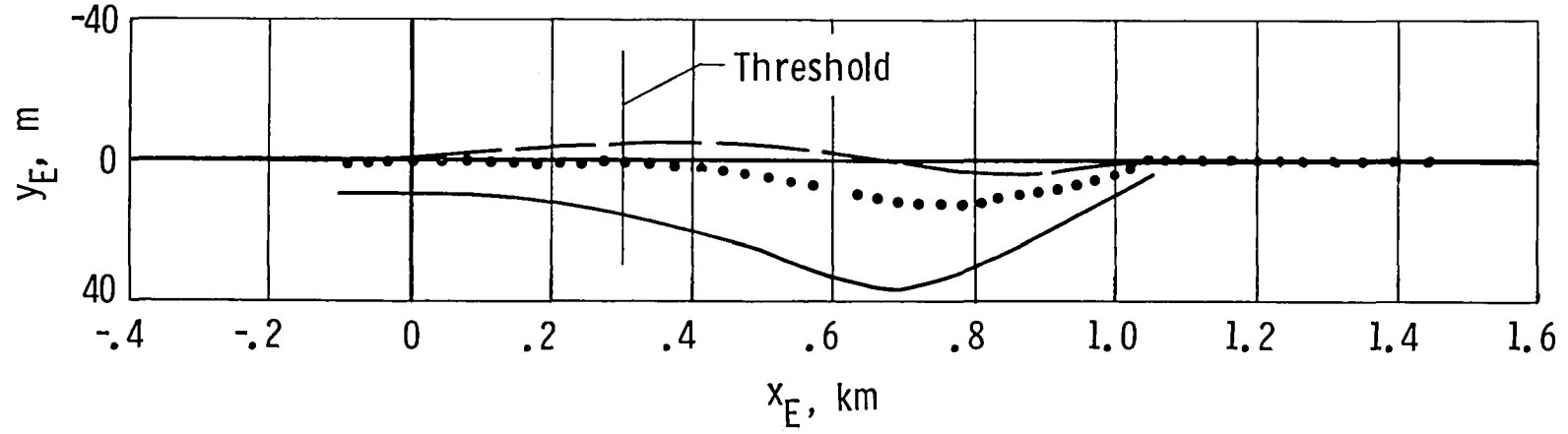

(a) Horizontal projection.

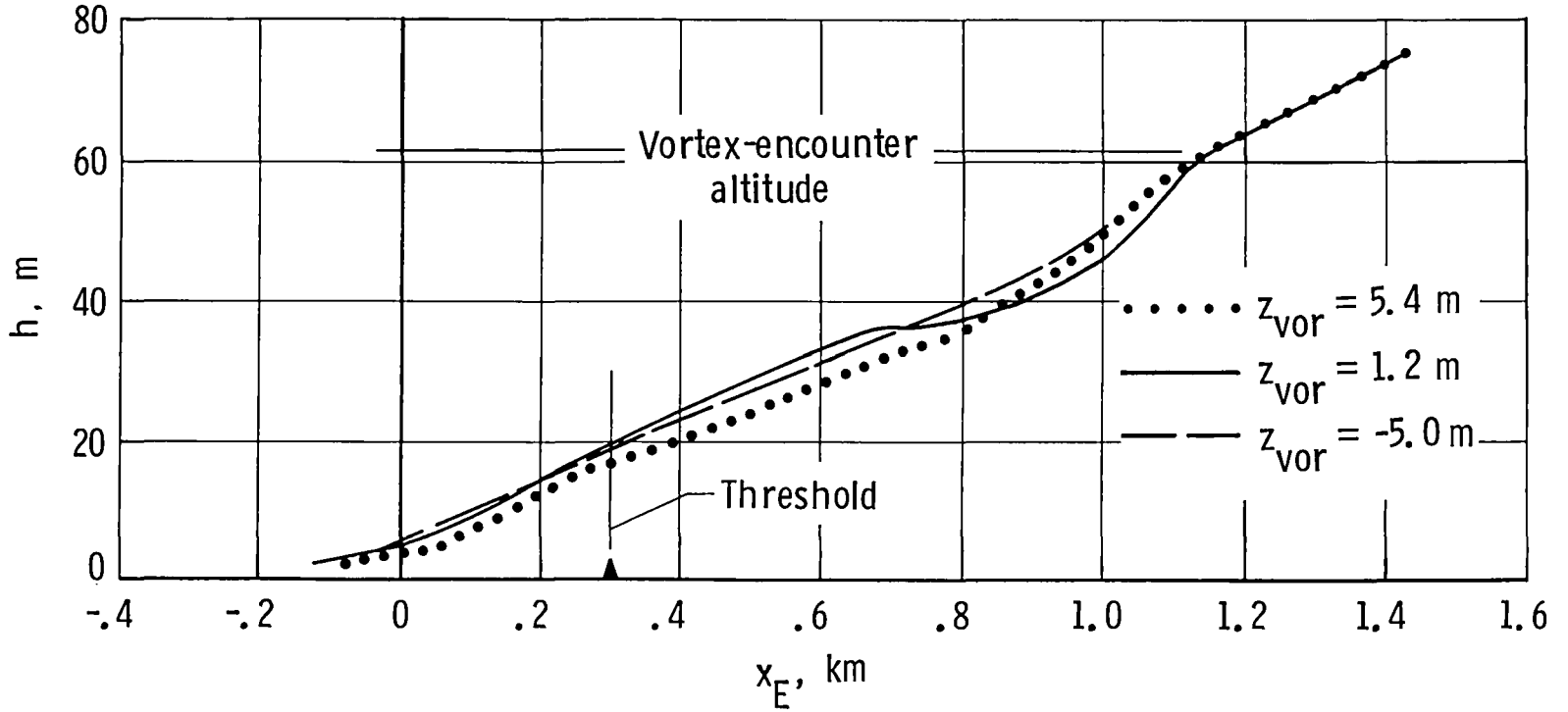

(b) Vertical projection.

Figure 15.- Effect of vertical location of vortex on flight path. Base-line vortex out of ground effect; T = 120 sec.

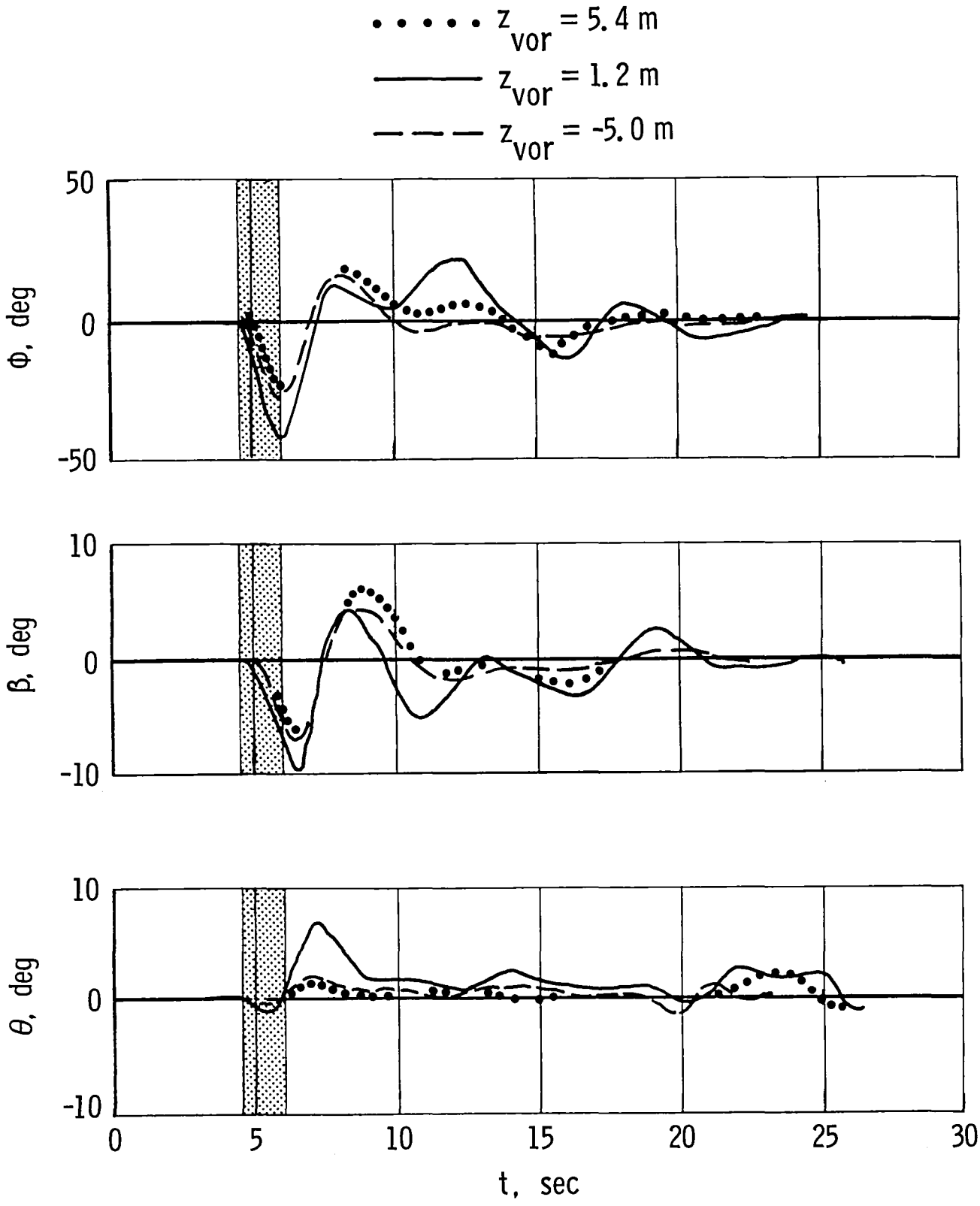

Figure 16.- Body attitude following piloted encounters with a vertically displaced vortex. Base-line vortex out of ground effect; T = 120 sec.

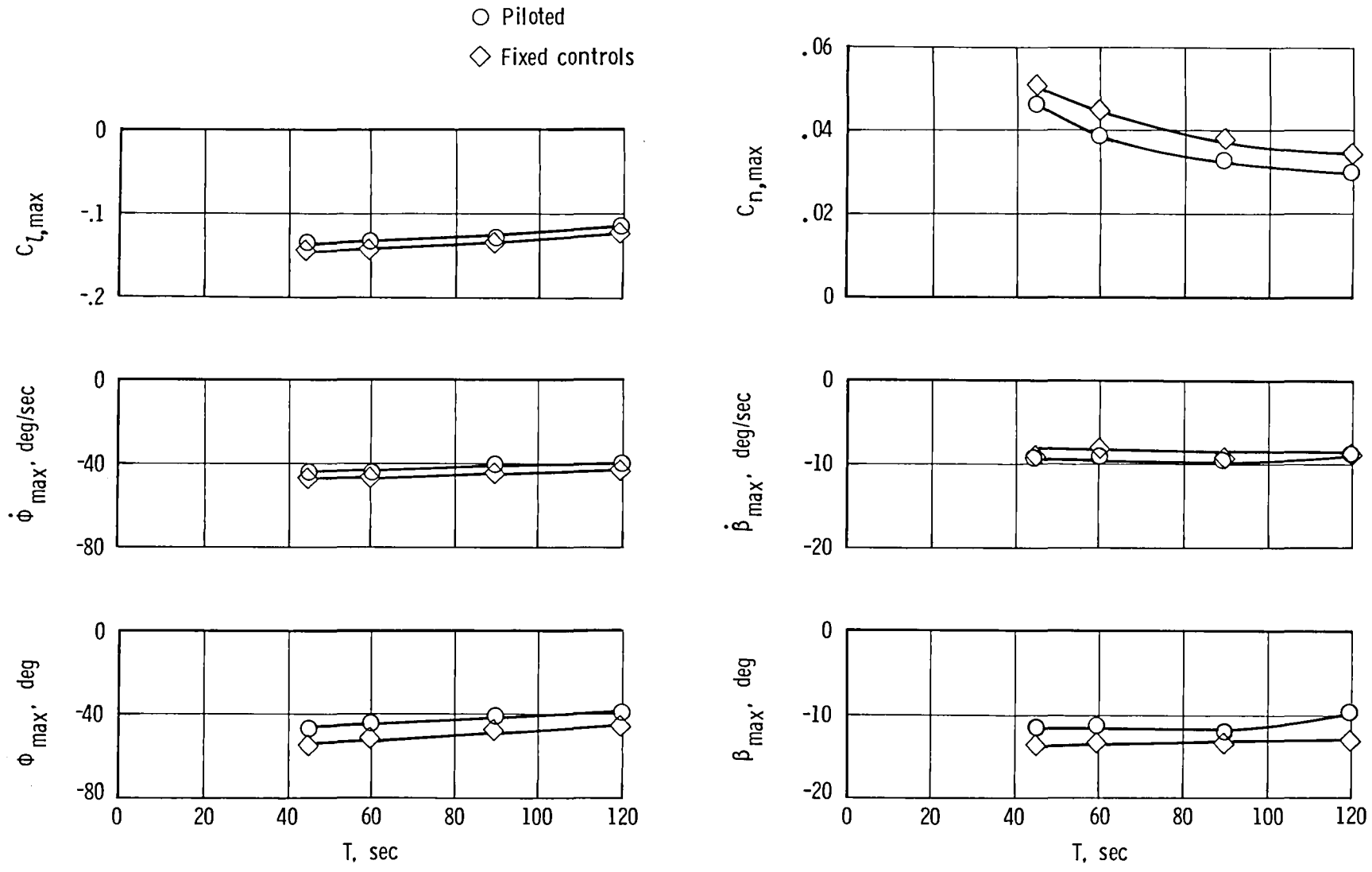

Figure 17.- Effect of vortex age on initial upset for encounters with base-line vortex out of ground effect.

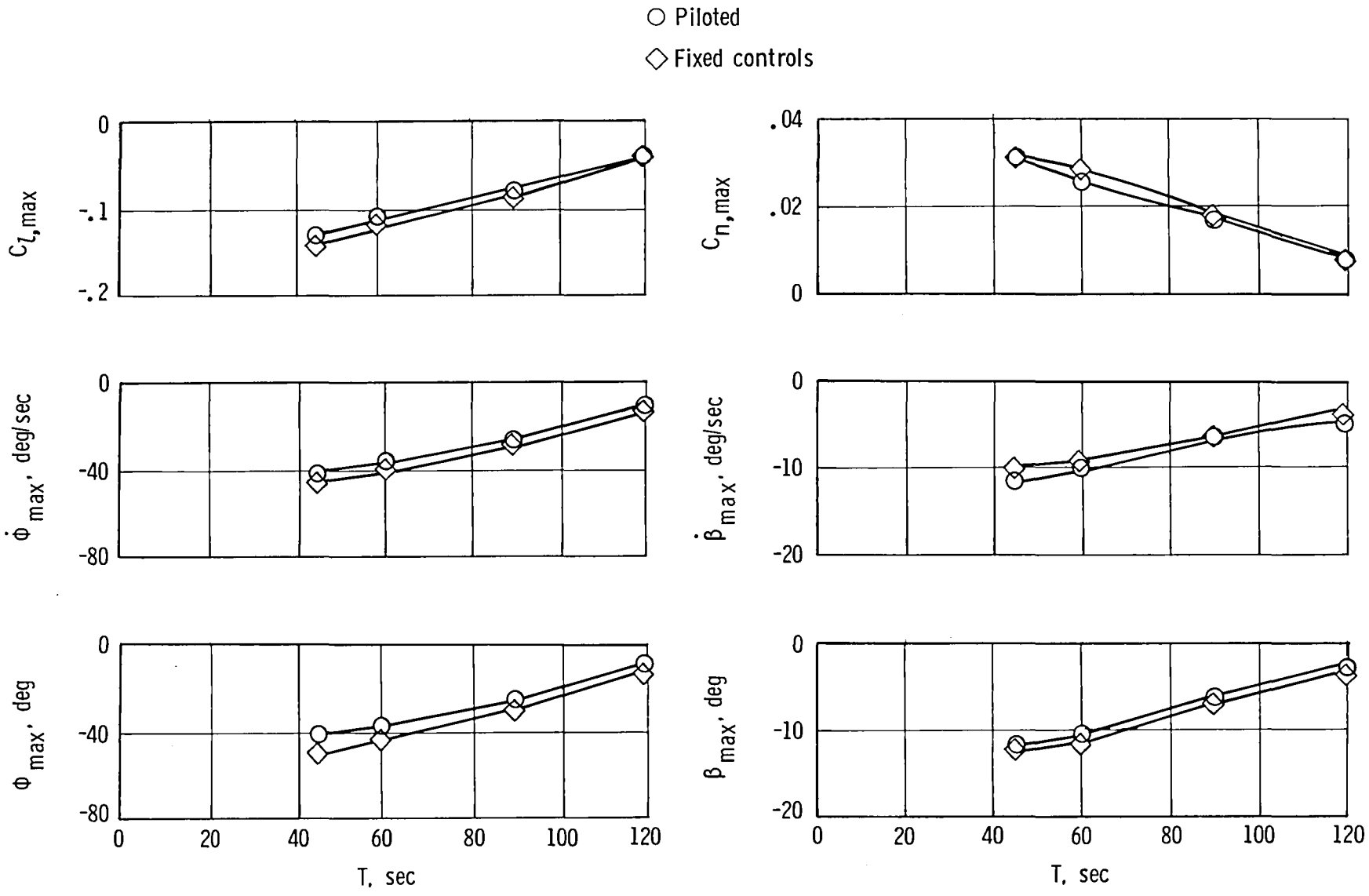

Figure 18.- Effect of vortex age on initial upsets for encounters with base-line vortex in ground effect.

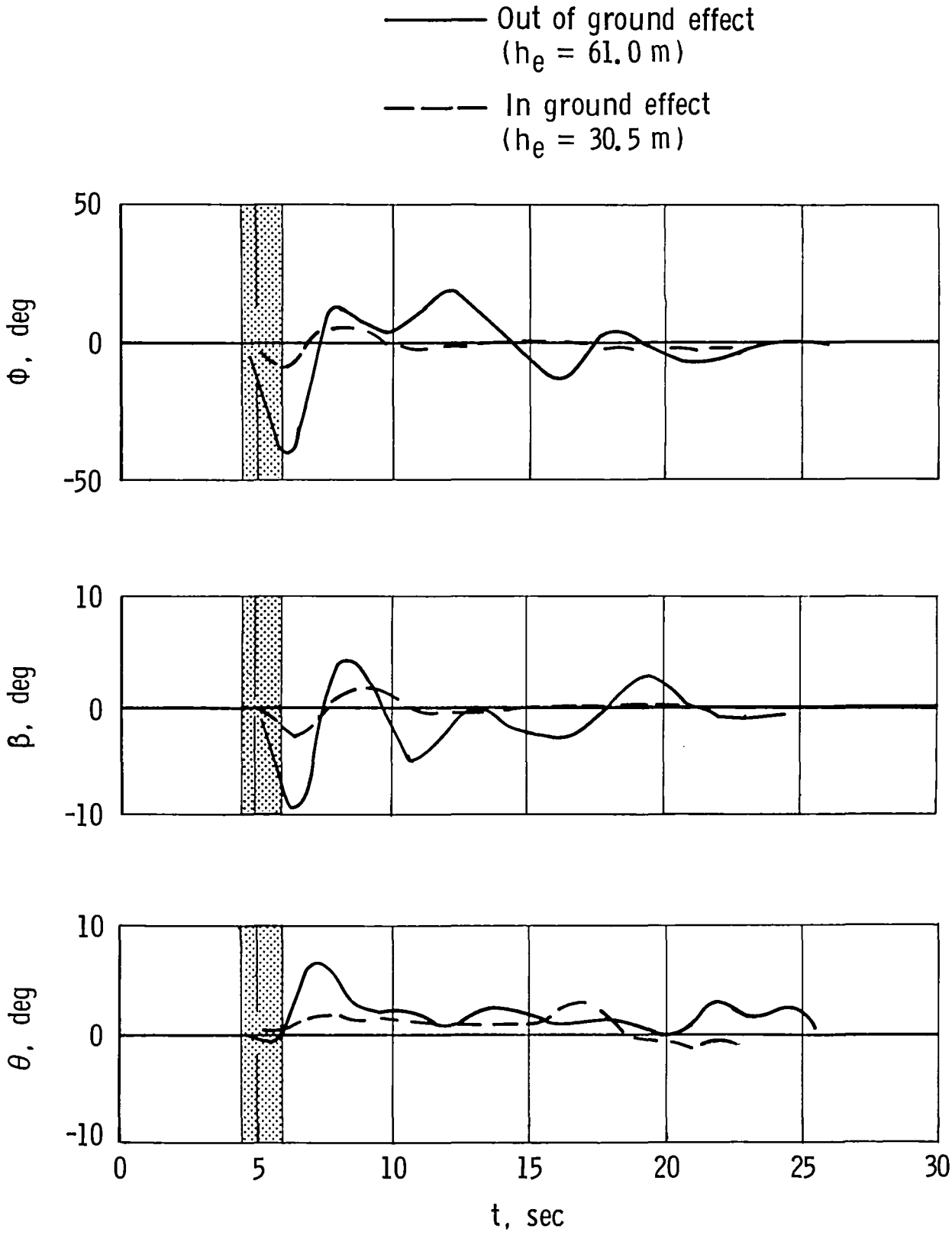

Figure 19.- Typical body attitudes following piloted encounters with the base-line vortex in and out of ground effect at an age of 120 sec.

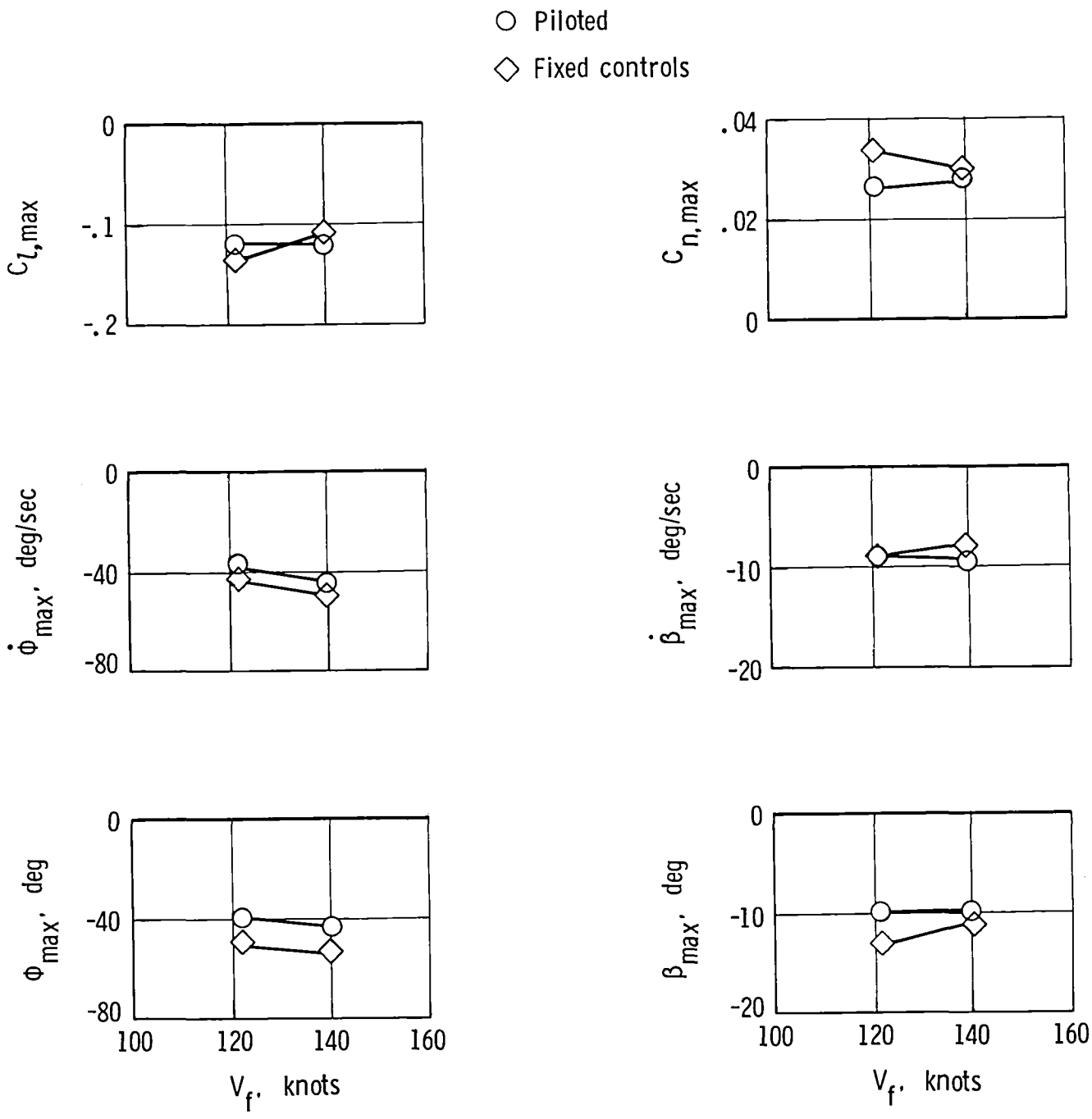

Figure 20.- Effect of speed of following airplane on initial response. Base-line vortex out of ground effect; T = 120 sec.

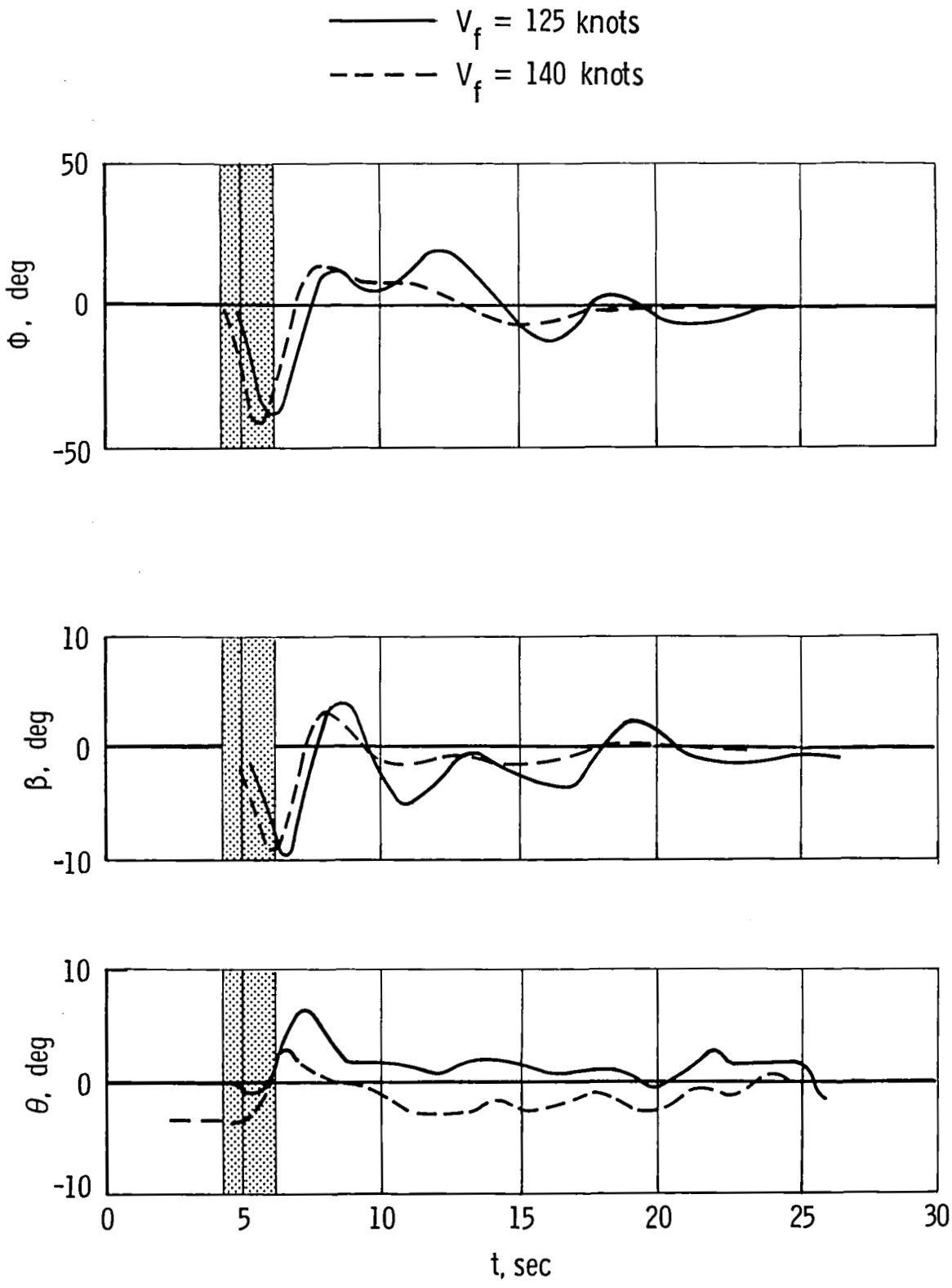

Figure 21.- Body attitudes following vortex encounters at several indicated airspeeds. Base-line vortex out of ground effect; T = 120 sec.

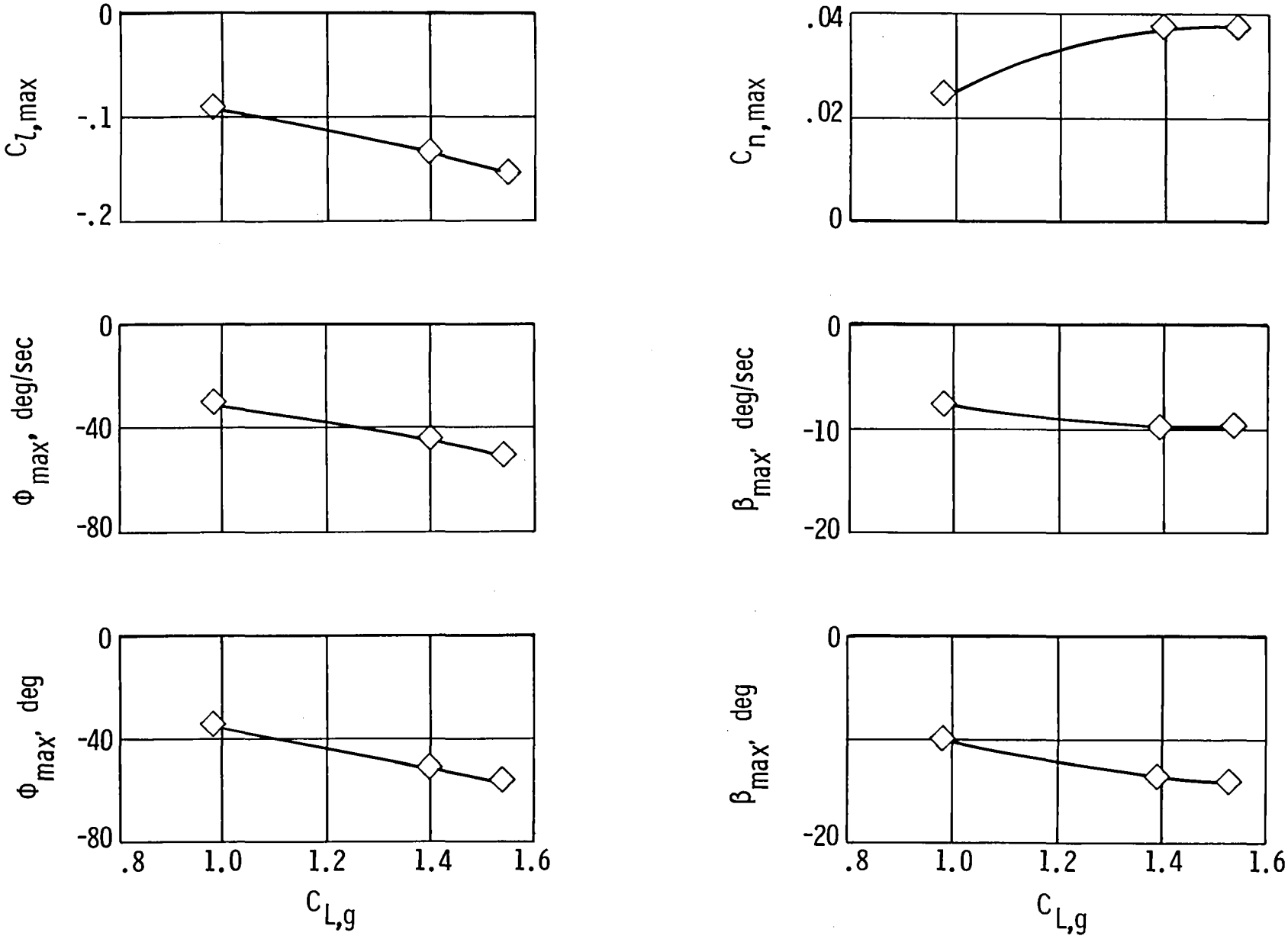

Figure 22.- Effect of lift coefficient of generating airplane on initial upset of following airplane with fixed controls. Base-line flow field out of ground effect; T = 120 sec.

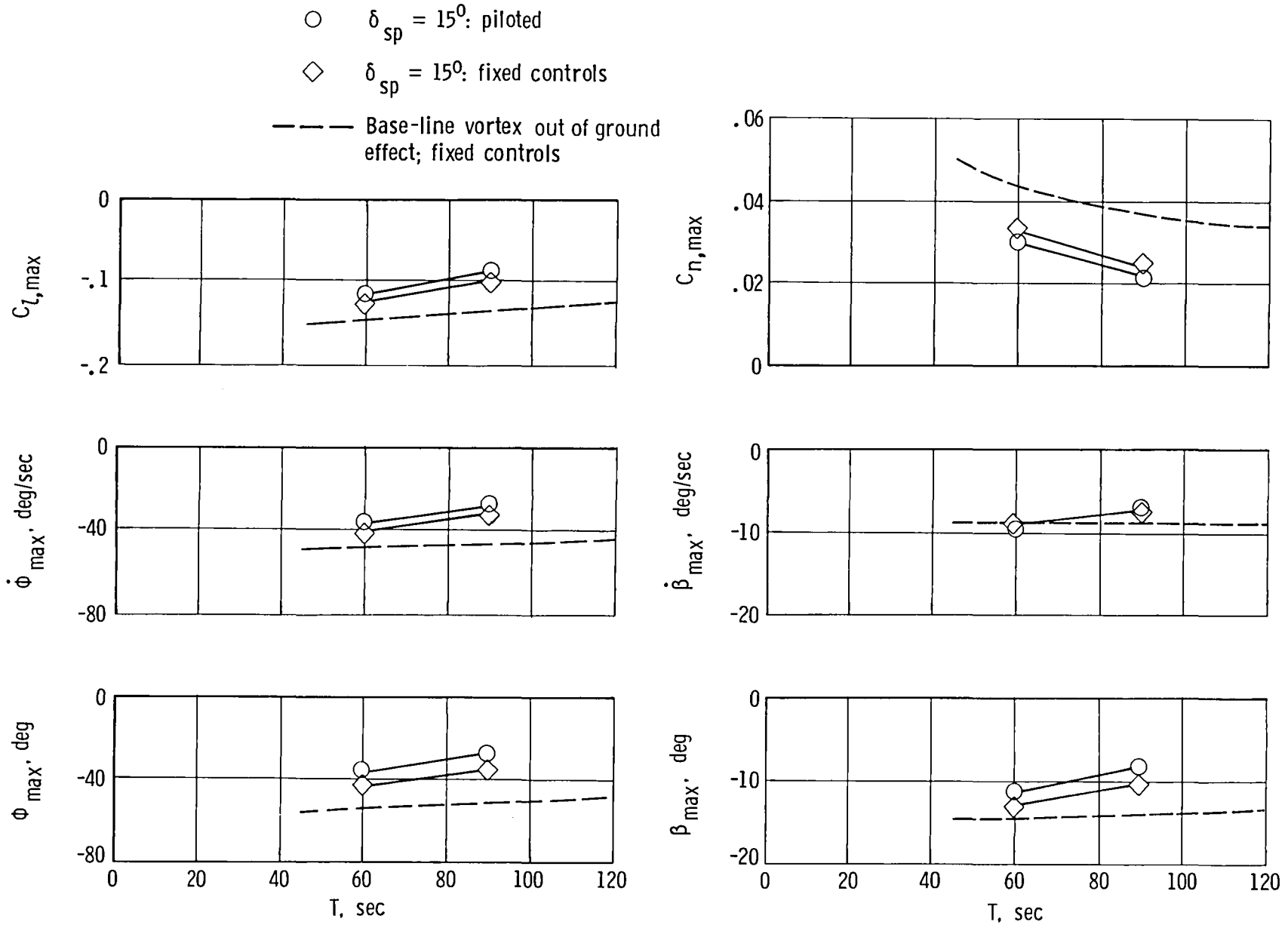

(a) Attenuated (δ_{sp} = 15°) flow field

Figure 23.- Effect of spoiler attenuation on the vortex generator on the following airplane initial responses.

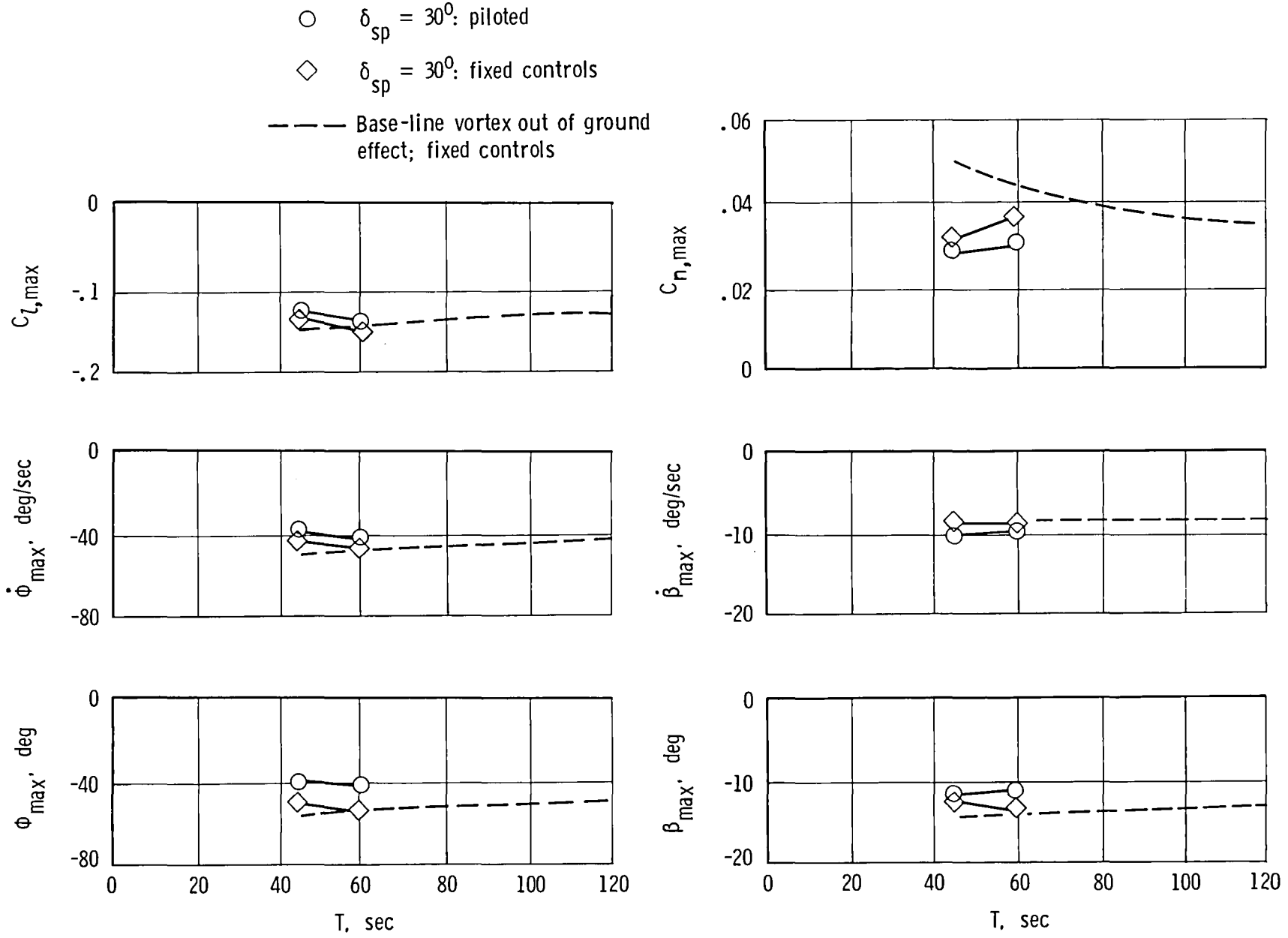

(b) Attenuated (δ_{sp} = 30°) flow field.

Figure 23.- Concluded.

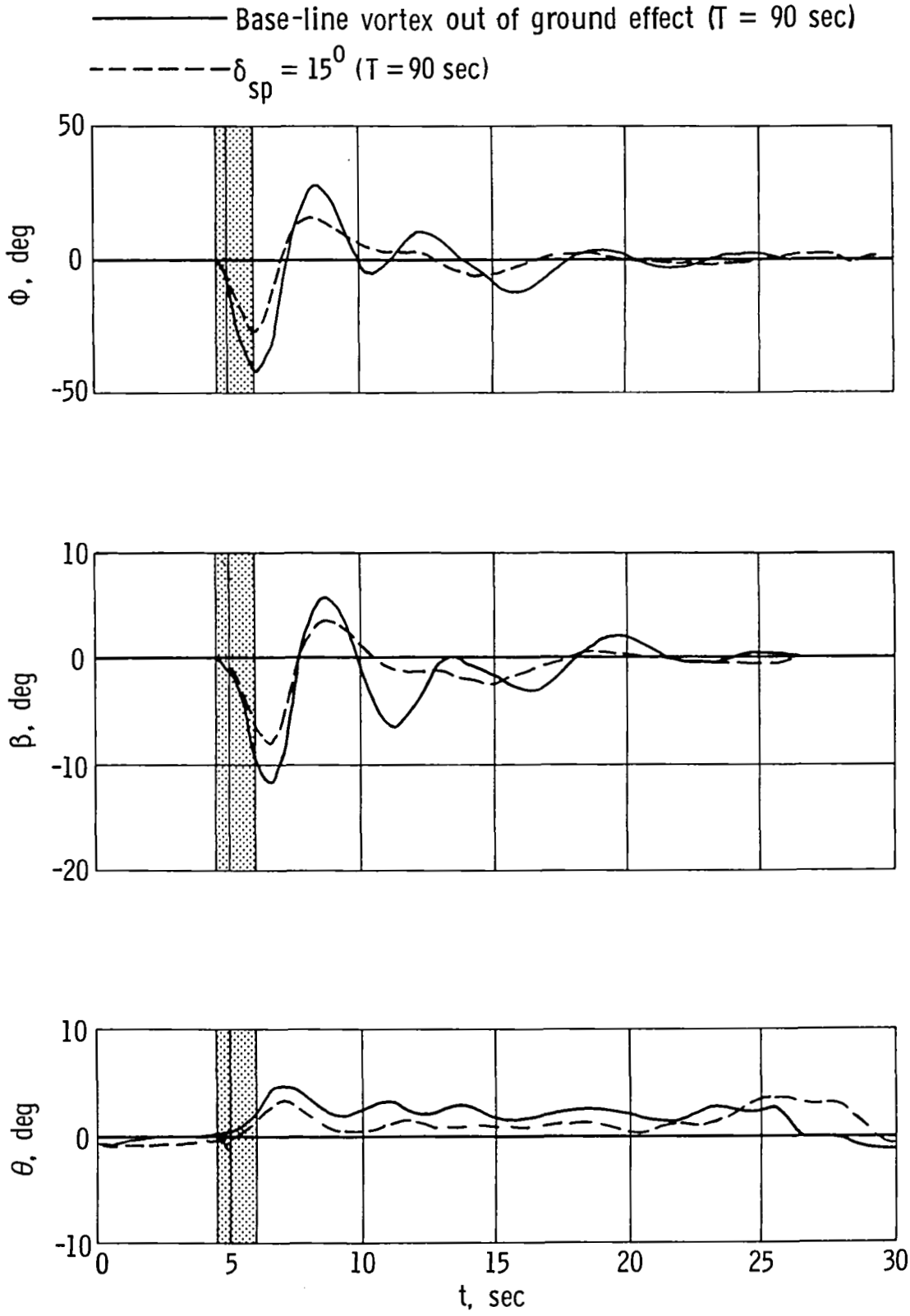

Figure 24.- Typical body attitudes following piloted encounters with the base-line flow field without spoiler attenuation and with 15° spoiler attenuation. T = 90 sec.

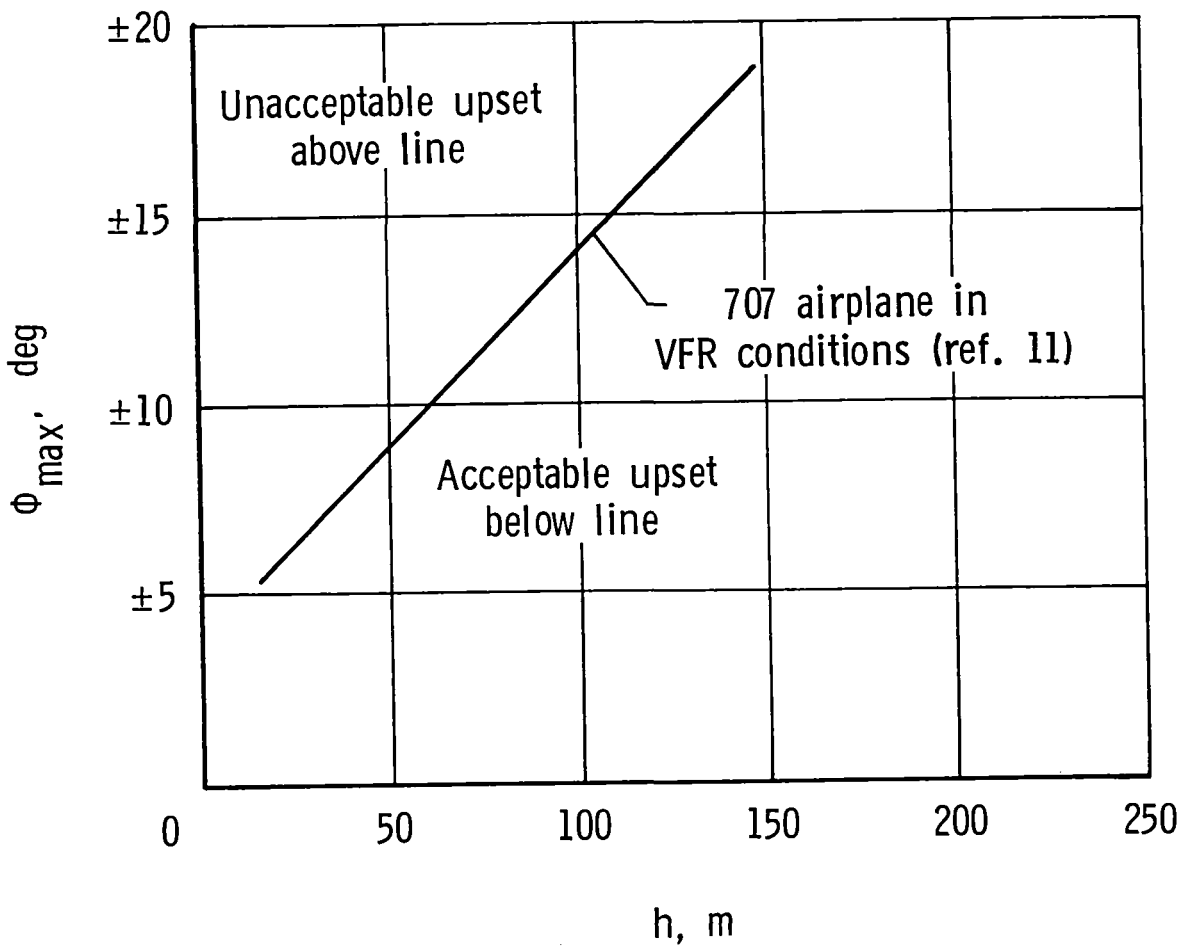

Figure 25.- Bank-angle criterion.

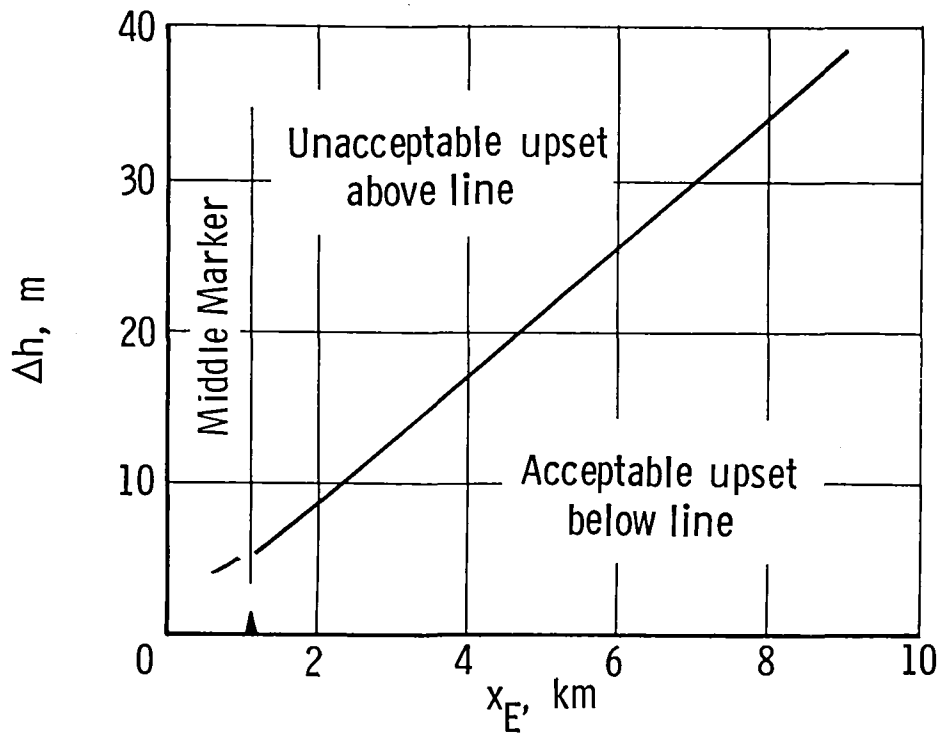

(a) Vertical-path deviation from glide slope.

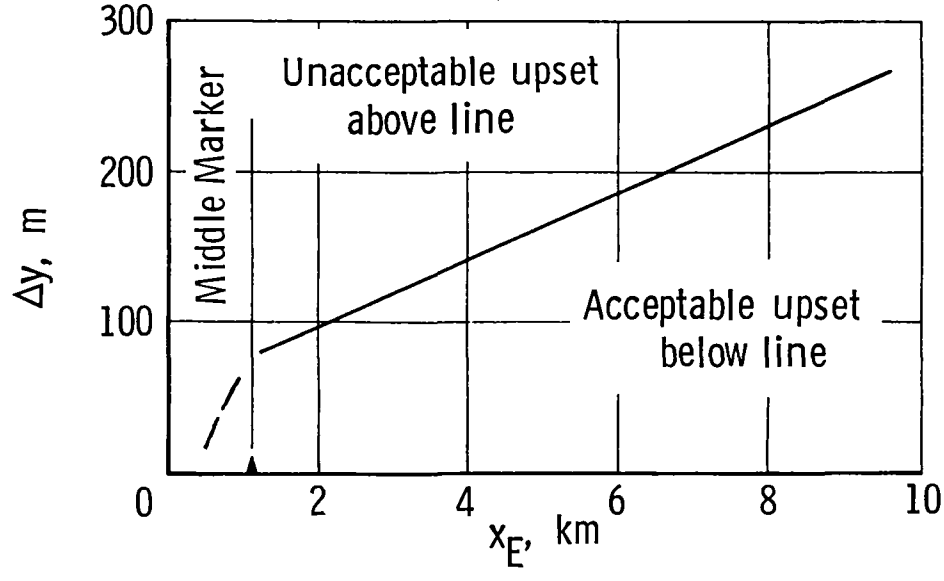

(b) Lateral-path deviation from localizer course.

Figure 26.- Flight-path excursion criterion.

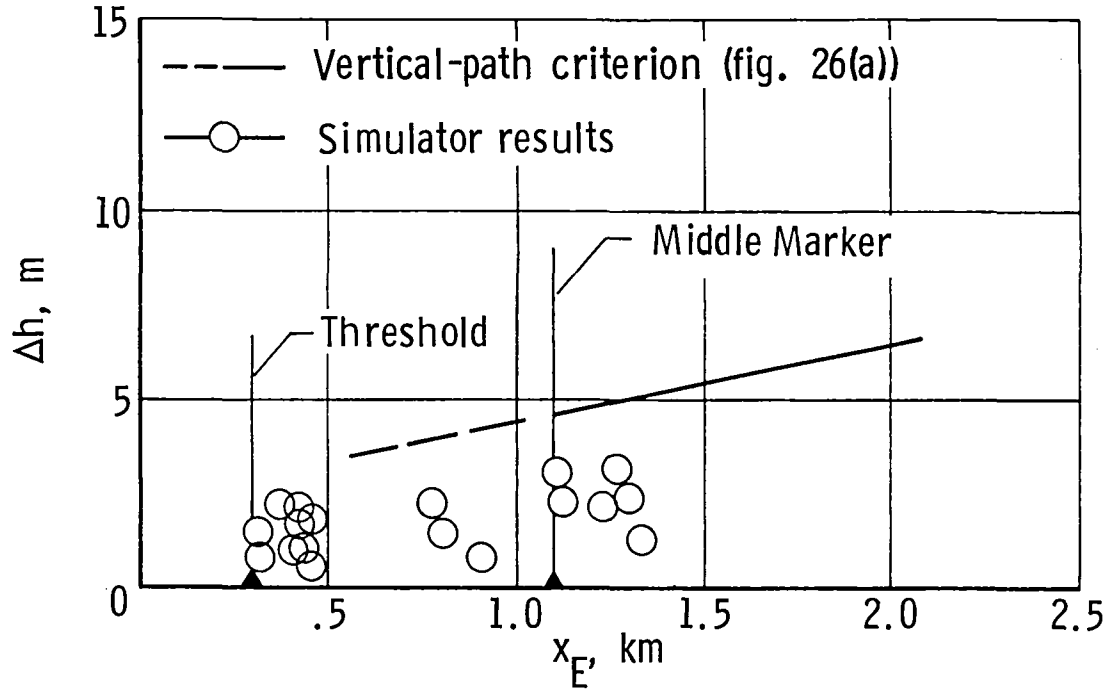

Figure 27.- Comparison of simulator results with vertical-path excursion criterion. Base-line vortex in ground effect; T = 120 sec.

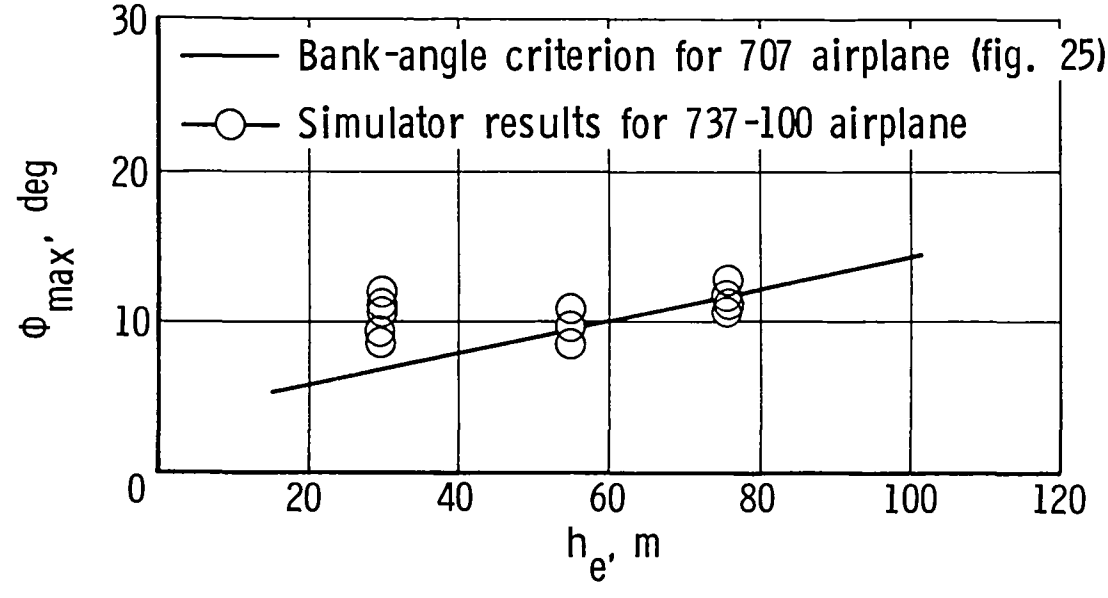

Figure 28.- Comparison of simulator results with bank-angle criterion. Base-line vortex in ground effect; T = 120 sec.

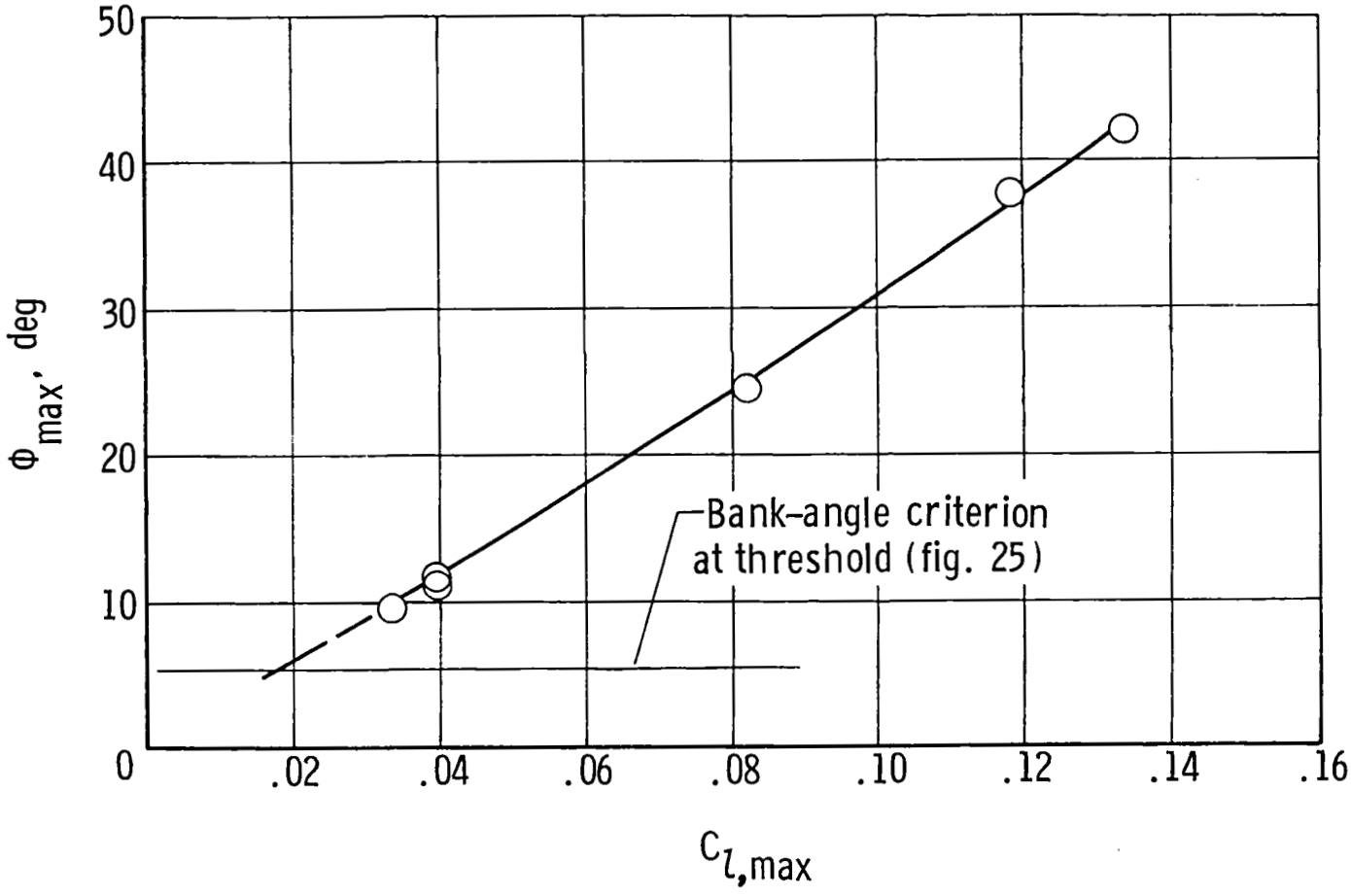

Figure 29.- Variation of maximum bank angle with rolling-moment coefficient. Piloted encounters; base-line vortex in ground effect.

1. Report No.	2. Government Accession No.	3. Recipient's Catalog No.
NASA TP-1966		

4. Title and Subtitle	5. Report Date
SIMULATOR STUDY OF VORTEX ENCOUNTERS BY A TWIN-ENGINE, COMMERCIAL, JET TRANSPORT AIRPLANE	February 1982
	6. Performing Organization Code: 505-31-93-02

7. Author(s)	8. Performing Organization Report No.
Earl C. Hastings, Jr., and Gerald L. Keyser, Jr.	L-14187
	10. Work Unit No.

9. Performing Organization Name and Address	11. Contract or Grant No.
NASA Langley Research Center Hampton, VA 23665	
	13. Type of Report and Period Covered: Technical Paper

12. Sponsoring Agency Name and Address	14. Sponsoring Agency Code
National Aeronautics and Space Administration Washington, DC 20546	

15. Supplementary Notes

Earl C. Hastings, Jr.: Langley Research Center.
Gerald L. Keyser, Jr. (Major): USAF, formerly of Langley Research Center.

16. Abstract

An investigation of vortex-induced upset and recovery characteristics was conducted by using a simulated twin-engine, commercial, jet transport airplane with fixed controls and with a conventional manual-control system. The piloted simulations were performed with the Langley Visual/Motion Simulator. Wake vortex encounters were simulated with the airplane in the final-approach configuration at altitudes between 76.2 m and 30.5 m. The investigation consisted of parametric studies of the effects of the lateral and vertical locations of the vortex center, vortex aging in and out of ground effect, approach speed of the simulated following airplane, lift coefficient of the vortex-generating airplane, and vortex attenuation by using the flight spoilers of the vortex-generating airplane. In addition, altitude-dependent bank angle and flight-path excursion criteria were used to evaluate the acceptability of the vortex-induced upsets.

17. Key Words (Suggested by Author(s))	18. Distribution Statement
Vortex encounters Flight management Dynamic stability Simulation	Unclassified - Unlimited Subject Category 08

19. Security Classif. (of this report)	20. Security Classif. (of this page)	21. No. of Pages	22. Price
Unclassified	Unclassified	63	A04

For sale by the National Technical Information Service, Springfield, Virginia 22161 NASA-Langley, 1982

National Aeronautics and
Space Administration

Washington, D.C.
20546

Official Business
Penalty for Private Use, $300

THIRD-CLASS BULK RATE

Postage and Fees Paid
National Aeronautics and
Space Administration
NASA-451

NASA

POSTMASTER: If Undeliverable (Section 158
Postal Manual) Do Not Return